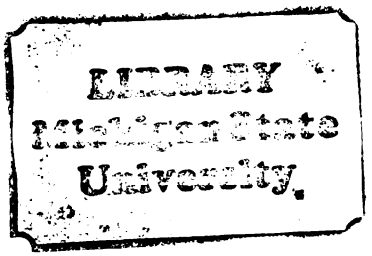

This is to certify that the

thesis entitled

Experimental Investigations on Age-Hardening
of Cu-10Ni-6Sn Spinodal Alloy

presented by

S. Shekhar

has been accepted towards fulfillment
of the requirements for

Masters degree in Metallurgy

K. N. Subramanian

Major professor

Date May 17, 83

EXPERIMENTAL INVESTIGATIONS ON AGE-HARDENING OF Cu-10Ni-6Sn SPINODAL ALLOY

By

Shekhar S.

A THESIS

Submitted to
Michigan State University
in partial fulfillment of the requirements
for the degree of

MASTER OF SCIENCE

Department of Metallurgy, Mechanics and Materials Science

1983

Shekhar S.

ABSTRACT

The dislocation structure in as-quenched and aged specimens of the Cu-10Ni-6Sn spinodal alloy, of both fine-grained and large-grained types, was studied by transmission electron microscopy. It was found that the deformation structure of aged specimens consisted of curved and wavy dislocations whereas deformed as-quenched specimens consisted of straight dislocations. This suggests that mixed dislocations may be responsible for the hardening during deformation of the spinodally modulated structure. It was seen that the dislocation density decreased with increased aging time; the dislocation multiplication seems to be hampered by the modulated structure. It was also observed that use of large-grained samples significantly aided in the analysis of the dislocation structure in the spinodally modulated alloys. The Burgers vector analysis of dislocations in an aged and deformed specimen indicated mixed dislocations to be responsible for the observed age hardening.

ACKNOWLEDGEMENTS

I would like to take this opportunity to sincerely thank my advisor Dr. K. N. Subramanian, but for whose constant guidance and encouragement this endeavour would not have ended in success. I would also like to say special thanks to my colleagues, Tong Lee and Apichart, my good friend Narendra, and scores of others in the Department of Metallurgy, who sacrificed a lot of their time and efforts to help me out.

This project is supported by the Department of Energy under Contract Number DE-AC02-81ER10942.

TABLE OF CONTENTS

LIST OF FIGURES

LIST OF TABLES

I. INTRODUCTION

Spinodal decomposition of alloys basically involves a periodic variation in space of local concentration of alloying elements. Such a modulation is sinusoidal in the early stages of the decomposition and square-shaped in the later stages. For a cubic system, the early stages of the decomposition can be expressed in terms of the following equation:

$$c - c_o = A \left(\cos \frac{2\pi}{\lambda} x + \cos \frac{2\pi}{\lambda} y + \cos \frac{2\pi}{\lambda} z\right) \qquad (1)$$

where,

c is the local atomic concentration of a secondary element,

c_o is the average atomic concentration of the secondary element,

A is an amplitude factor, and

λ is the wavelength of the composition modulation.

For a cubic system in general, the x, y and z axes are parallel to the <100> directions.

The modulation caused by the decomposition during the aging of a spinodal alloy accounts for increases in the yield and flow stresses of the alloy, and this is termed as age-hardening. In this investigation the nature of the dislocations in aged and deformed specimens of the spinodal alloy was studied to gain a better understanding of the mechanism of age-hardening in spinodally modulated structures.

The Cu-10Ni-6Sn spinodal alloy was chosen for the experimental work on the basis of its cubic structure, the relative ease in controlling at desired stages of decomposition and as well as on the basis of the availability of experimental data for mechanical properties in bulk specimens.

II. LITERATURE SURVEY

2.1 Theory of Spinodal Decomposition

The spinodal phase has long been regarded as a limit beyond which a homogeneous phase could no longer be metastable (1). But recently it has become apparent that a phase beyond the spinodal phase would decompose by simple diffusional clustering mechanism which is quite different from the nucleation and growth mechanisms encountered for metastable phases. The theory of spinodal decomposition, which is based on the diffusion equation modified by thermodynamic requirements, is phenomenological, and each parameter can be measured by independent thermodynamic or diffusion experiments.

The variation of the Helmholtz free energy F with composition at a temperature T_o is considered in a binary alloy system, as shown in Figure 1(a). The two inflection points C_{S1} and C_{S2} are defined by

$$\left(\frac{\partial^2 F}{\partial C^2}\right)_{T,v} = F'' = 0 \qquad (2)$$

where,

C is the atomic concentration of the second component,

and v is the volume of the binary alloy.

The point $C_{\alpha 1}$ and $C_{\alpha 2}$ are points of common tangency to the curve and they define the composition of the co-existing phases at T_o. The locus of points satisfying Equation 2. for different temperatures is called the spinodal (chemical spinodal) and is shown by the dashed

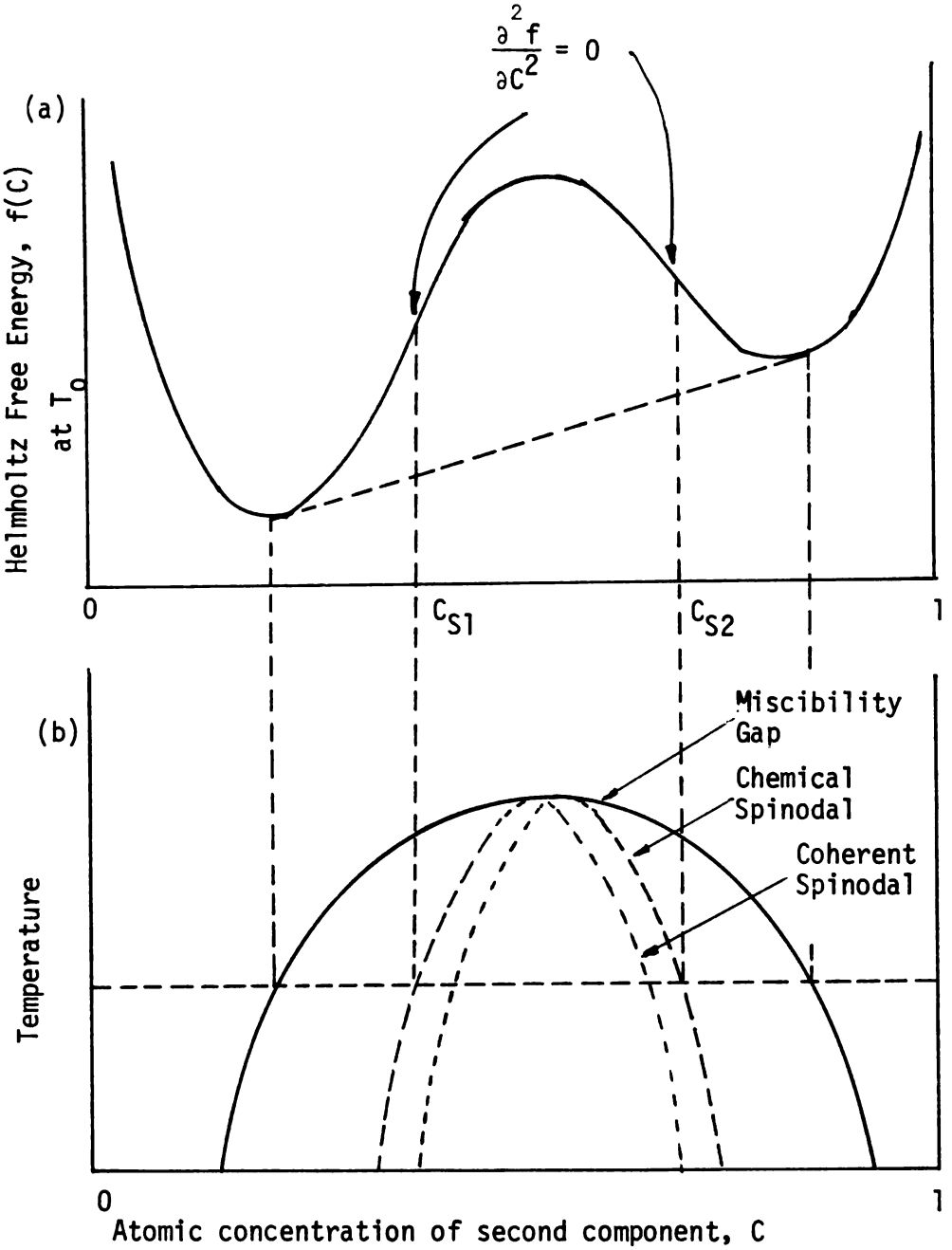

Figure 1 : a) The free-energy versus composition curve at temperature T_o.

b) Binary alloy phase diagram with miscibility gap, chemical spinodal and coherent spinodal.

curve in Figure 1(b). The locus of the points $C_{\alpha 1}$ and $C_{\alpha 2}$ for different temperatures is the solid line in Figure 1(b) and this line represents the miscibility gap. The significance of the spinodal line is as follows: alloys which become supersaturated by cooling from the single phase solid solution region to the two phase region inside the miscibility gap will nucleate precipitates whose morphology and distribution depend markedly on whether the alloy is inside or outside the spinodal line. For an alloy which lies between the phase boundary and the spinodal line, the second derivative of the Helmholtz free energy with respect to composition, $\frac{\partial^2 F}{\partial C^2}$, is positive and there will be a nucleation barrier to precipitation, that is, the alloy is stable to small composition fluctuations. For alloys which lie inside the spinodal line, $\frac{\partial^2 F}{\partial C^2}$ is negative, there is, in principle, no nucleation barrier to precipitation and the alloy is unstable to small composition fluctuations (3).

Although spinodal decomposition was recognized by Gibbs (4), it is only recently that the theory of this type of precipitation has been developed by Hillert (5), and Cahn and Hilliard (6, 7) to an extent where it can be used to predict microstructural behavior. These authors have shown that a solid solution inside the spinodal is unstable to sinusoidal fluctuations of wavelength $2\pi/\beta$ when:

$$\frac{\partial^2 f'(C)}{\partial C^2} + 2k\beta^2 + \frac{2\eta^2 E}{(1-\nu)} < 0 \qquad (3)$$

where, f'(C) is the free energy of a unit volume of a homogeneous material of composition C, k is a constant determined by the surface

energy between the two phases, E is Young's modulus, ν is the Poisson's ratio, and η is the linear expansion of the lattice per unit composition change.

Thus the pure thermodynamic condition for spinodal decomposition ($\frac{\partial^2 f'(C)}{\partial C^2} < 0$) is modified by the second and third terms in Equation 3 which represent respectively, the energy barriers due to the creation of an additional area of interface in the lattice, and to the volume strain energy of the misfitting phases. It can be seen that for given values of $\frac{\partial^2 f'(C)}{\partial C^2}$ and η, there will be a certain maximum value of β to satisfy the Equation 3 and hence a certain minimum value of the wavelength of composition into which the alloy can decompose. All composition fluctuations having wavelength above this critical value, λ_c, are also stable; but Cahn (7) has shown that the wavelength which grows most rapidly, and hence the one which is probably observed experimentally, is $\sqrt{2}\,\lambda_c$. The presence of a strain energy term means that the decomposition takes account of the elastic anisotropy of the crystal lattice since E is a minimum along <100> in most cubic metals, three orthogonal fluctuations along <100> directions are preferred. The microstructural result of this is a distribution of second phase particles which consists of an ordered array of approximately spherical particles for small volume fractions of precipitates and an array of rods along <100> directions for larger volume fractions.

In order to account for the effect of coherency strains, Cahn (7) introduced an additional term in Equation 2.

$$F'' + 2\eta^2 y = 0 \qquad (4)$$

where Y, in the case of <100> modulations, can be expressed in terms of the elastic constants C_{ij} as

$$Y = C_{11} + C_{12} - 2\,(C_{12}^2/C_{11}). \qquad (5)$$

The locus of points satisfying Equation 4, which always lies inside the chemical spinodal, is defined as the coherent spinodal, and is shown in Figure 1(b).

The initial kinetics and mechanism of spinodal decomposition in cubic crystals has been completely described by Cahn (8) in terms of the seven parameters $\partial^2 f'(c)/\partial c^2$, k, M, η and the three elastic constants C_{44}, C_{11} and C_{12}, where k is the gradient energy co-efficient, and M is the mobility of atoms. According to Cahn (8), the initial kinetics and mechanism is completely independent of crystal structure. Of the above parameters, all but $\partial^2 f'(c)/\partial c^2$ and k can be readily determined by extrapolation of free energy data and k has been estimated (6) from statistical mechanics.

The following predictions may be made of the initial stages of spinodal decomposition:

(i) If $(2C_{44} - C_{11} + C_{12}) > 0$, spinodal decomposition should give composition fluctuations primarily on all three {100} planes. If $(2C_{44} - C_{11} + C_{12}) < 0$, these should lie about the four {111} planes.

(ii) The initial kinetics of decomposition are described by an exponential increase (or decrease) in amplitude of each Fourier component. For a given composition and temperature the amplification factor as a function of wavelength and

orientation is completely described by $\partial^2 f'(c)/\partial c^2$, k, M, η, C_{44}, C_{11} and C_{12}.

(iii) The kinetics are such that after a while the fastest growing composition fluctuations predominate giving rise to almost pure sinusoidal fluctuations which lie on the <100> or <111> directions and have a wavelength $\sqrt{2}$ times the critical wavelength ($2\pi/\beta_c$).

(iv) The kinetics and wavelengths of the fastest growing composition fluctuations as a function of temperature and composition are described by the temperature and composition dependence of the various parameters.

(v) The limit of metastability in aeolotropic cubic crystals occurs sooner than one would expect. The spinodal decomposition mechanism seeks out the plane where the modulation occurs most easily.

(vi) Since various composition fluctuations do not interact with each other, the structure at the initial stages will be approximately represented by the composition fluctuations along the three {100} planes or the four {111} planes. The former resembles a simple cubic array of regions rich in one component connected along the <100> directions by rods similarly enriched. The body centers of this array are regions depleted in this component connected by similarly depleted <100> rods.

It is possible to make some qualitative predictions about the later stages of spinodal decomposition:

(i) When the amplitude of the plane waves becomes such that the higher order terms in the expansion of $f'(C)$ about C_o become imporant, there will be an interaction (7) among the composition fluctuations in the different planes which causes a slowing down of the rate of growth to the equilibrium composition, and distorts the fluctuations in the different planes.

(ii) Depending on the relative volumes of the two phases in equilibrium, imperfect versions of the following morphology are expected:

a) If the volume fraction of one phase is much smaller than the other, the {100} habit will give a simple cubic array of octahedral particles whose corners are aligned along the <100> directions.

b) The {111} habit will give a face-centered cubic array of particles of the minor phase. These particles should vary from spheres to cubes as the volume fraction increases.

(iii) The initial spacing of the particles in the {100} habit is equal to the wavelength of the most rapidly growing composition fluctuation; in the {111} habit, the near neighbor spacing of particles (in the <110>) is $\sqrt{\frac{3}{2}}$ times the wavelength of the most rapidly growing fluctuation.

(iv) During the initial stages, the amplitude of the individual composition fluctuations is only about one third for the {100} habit (or one fourth for the {111} habit) of the maximum

composition difference in the sample. A similar fraction persists as long as coherency is maintained, so that the observed separation of the side bands in x-ray diffraction patterns which are due to local composition differences in the modulated structure, will represent only a fraction of the actual composition difference.

(v) The maximum elastic shear strain is at the corners of the particles (octahedral particles for the {100} habit, and spherical to cubic particles for the {111} habit) and is of the order of the fractional lattice parameter difference.

(vi) The reported increase in wavelength with time is probably due to resolution of some of the particles or rods and growth of others. The driving force for it is the reduction in surface-free energy.

In conclusion, it must be said that spinodal decomposition differs from nucleation and growth in that it proceeds from a stage small in degree but large in extent, passing through stages of primarily increasing amplitude, whereas a nucleation and growth mechanism proceeds from a stage small in extent but large in degree, passing through stages of primarily increasing extent. In spinodal decomposition there is no clear division where one can say the new phase has appeared; in nucleation and growth this is the important nucleation event.

2.2 Mechanical Properties in Spinodal Alloys

There have been extensive investigations on the role of long-range coherent composition fluctuations resulting from spinodal decomposition

on mechanical properties of cubic crystals. One of the first theoretical studies of this nature was done by Cahn (9), who considered first a single Fourier component of the composition fluctuations Δc whose wave vector β is in the [001] direction and whose amplitude is $A(\beta)$. According to Cahn (9),

$$\Delta c = c - c_o = A(\beta) \cos\beta z \tag{6}$$

where c_o is the average composition. The internal stress components σ_{ij} produced by this plane composition fluctuation is given by

$$\sigma_{xx} = \sigma_{yy} = (\eta \Delta c Y) = A\eta Y \cos\beta z \tag{7}$$

$$\sigma_{zz} = \sigma_{xy} = \sigma_{yz} = \sigma_{zx} = 0.$$

The force $\vec{F}$ on a dislocation per unit length produced by a stress field $\tilde{\sigma}$ is

$$\vec{F} = (\vec{b}.\tilde{\sigma}) \times \hat{\xi} \tag{8}$$

where, $\vec{b}$ is the Burgers vector, and $\hat{\xi}$ is the unit tangent to the dislocation line. The force on a dislocation line is always perpendicular to $\hat{\xi}$ and for edge dislocations consists of both climb and glide components. The glide component $\vec{F}_g$ is given by

$$\vec{F}_g = (\hat{n}x\hat{\xi}) \ (b\tilde{\sigma}n) \tag{9}$$

where $\hat{n}$ is the unit normal to the glide plane. Equation 9. applies equally well to screw dislocations but since these can glide on a number of planes it is sometimes convenient to use Equation 8,

which for screw dislocations becomes

$$\vec{F} = -\frac{1}{|\vec{b}|} (\vec{b}.\tilde{\sigma}x\vec{b}). \tag{10}$$

In inhomogeneous alloys there exist several other sources of forces on dislocations that are not present in a homogeneous alloys of the same composition and these relate mainly to the composition gradients. For very small gradients the self-energy γ of a dislocation is approximately given by

$$\gamma \simeq Gb^2 \sim \gamma b^2 \tag{11}$$

where G is the shear modulus.

If γ varies with position there will be a force on the dislocation (10, 11) given by

$$\vec{F}_c = -\hat{\xi}x(\vec{grad}\ \gamma\ x\hat{\xi})$$

$$= \gamma(\frac{d\ell nG}{dc} + 2\eta)\ (\vec{\nabla}cx\hat{\xi})x\hat{\xi}. \tag{12}$$

The corresponding glide force on a plane whose unit normal is $\hat{n}$ is

$$\vec{F}_{cg} = -\gamma\ (\frac{\partial\ell nG}{\partial c} + 2\eta)\ (\vec{\nabla}cx\hat{\xi}.\hat{n})\ \ (\hat{\xi}x\hat{n})\ . \tag{13}$$

Another source of forces in a gradient comes from the fact that after slip through an inhomogeneous region, the two opposing faces now differ in composition given by

$$\Delta c = \vec{b}.\ \vec{grad}\ c\ \ . \tag{14}$$

Cahn (9) considered the forces on dislocations in the {111} $\langle 1\bar{1}0\rangle$ slip system, which interacts with only two of the three fluctuation components. It should, therefore, behave as if the sample contained an assembly of pseudo-rods along [001]. In this case, the slip plane cuts across the rods and all parallel {111} planes encounter the same set of obstacles as do the $\{11\bar{1}\}$ cross-slip planes.

Consider the equation of the slip plane to be

$$x + y + z = \sqrt{3}\, d \tag{15}$$

where the cartesian coordinates x, y and z are parallel to the <100> directions, and d is the distance from the slip plane to the origin. Rotating the [XYZ] coordinate system to [X'Y'Z'] such that X' is along $[1\bar{1}0]$ and Y' is along $[11\bar{2}]$ in the slip plane, will provide the following expression

$$\begin{aligned} \sqrt{2}\, x' &= x - y \\ \sqrt{6}\, y' &= x+y - 2z + 2\sqrt{3}d \quad . \end{aligned} \tag{16}$$

By virtue of Equation 15,

$$\sqrt{6}y' = 3x + 3y \quad . \tag{17}$$

So that the resolved force on a $[1\bar{1}0]$ dislocation is

$$\vec{b}.\tilde{\sigma}.\hat{n} = \frac{2}{3} A\eta|b|\, y \sin\left(\frac{1}{\sqrt{6}} \beta y'\right) \sin\left(\frac{1}{\sqrt{2}} \beta x'\right). \tag{18}$$

The (111) slip plane thus resembles a rectangular checkerboard of alternating forces, as shown in Figure 2. The sides of the rectangles are the locus of zero force positions and within each rectangle the force rises or falls to an extremum in the center.

Problems of the above nature have two extremes: If $A\eta|b|y/\gamma\beta<1$, the dislocation line is almost straight and if $A\eta|b|y/\gamma\beta>1$, the dislocation curves around all obstacles.

Cahn (9) therefore, predicted that age-hardening in spinodal alloys is due to the motion of edge and screw dislocations. He has predicted that the yield stress varied as $A^2\lambda$. Explicitly, he has stated that at applied stresses exceeding $\frac{A^2\eta^2y^2b}{3\sqrt{6}\beta\gamma}$ for screws, and $\frac{A^2\eta^2y^2b}{\sqrt{2}\beta\gamma}$ for edges, the dislocations should move continuously through the structure. But the major drawback of Cahn's theory is that experimentally obtained values of yield stress for spinodally modulated structures are very much higher than theoretically predicted values, as noted by Douglass and Barbee (12), Ditchek and Schwartz (2) and Lefevre et al (13). Moreover, the predicted $A^2\lambda$ dependence of the yield stress is not applicable, as noted by Butler and Thomas (14) and Lefevre et al (13).

Carpenter (15) and as well as Ditchek and Schwartz (16) considered lattice-mismatch theories to explain the age hardening mechanism in spinodally modulated structures. They considered the mismatch between the lower and upper half of a slip plane due to the difference in the lattice parameter when a dislocation cuts through the modulated structure. For example, in the experimental work on 60Au-40Pt alloys, Carpenter (15) has considered the alloy lattice

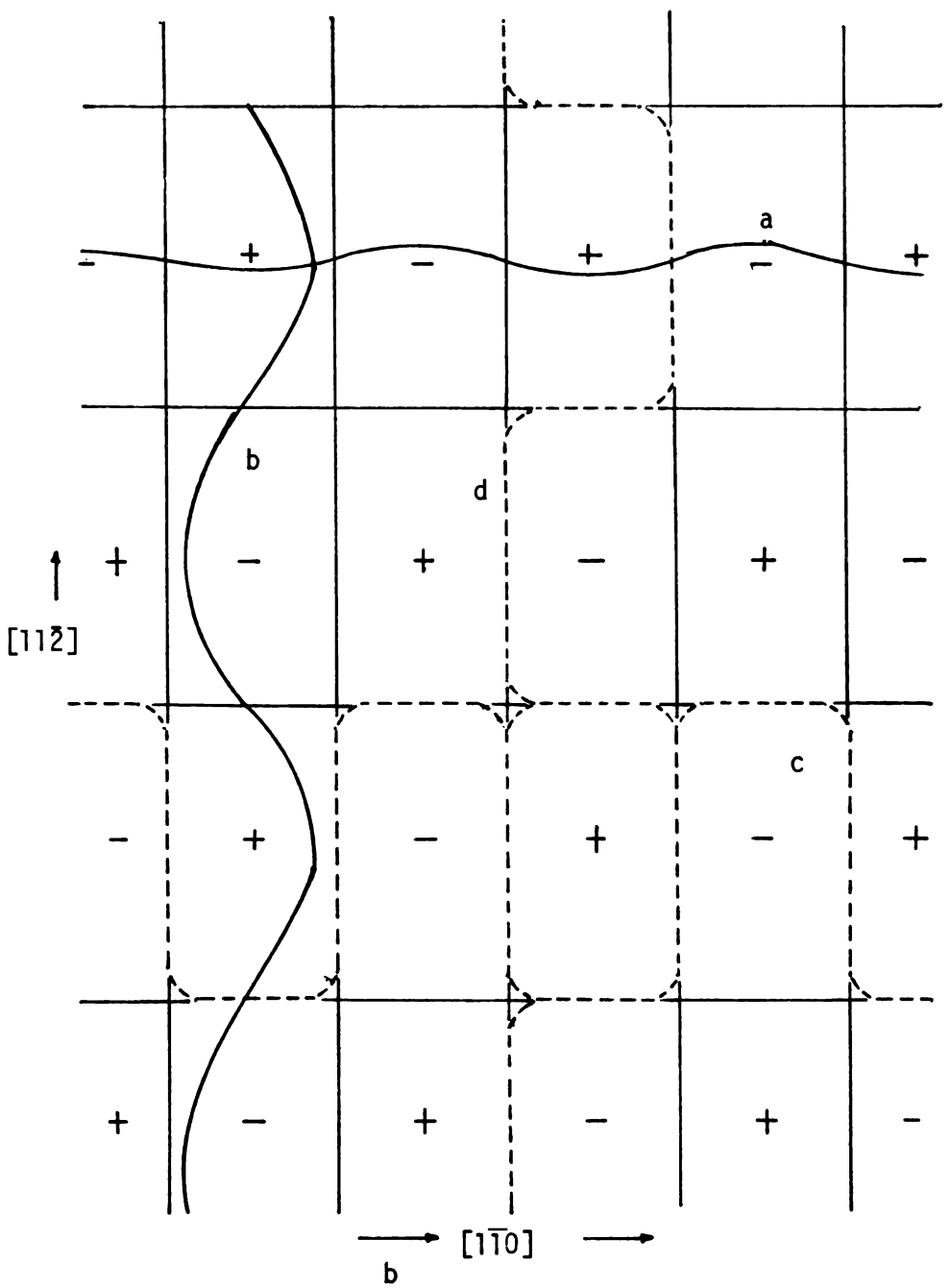

Figure 2: The (111) [1$\bar{1}$0] slip system in the absence of applied stress showing the forces on the dislocation and the resulting configurations (9)

a) screw at small amplitude for that wavelength,

b) edge at small amplitude for that wavelength,

c) screw at large amplitude, and

d) edge at large amplitude.

to be a sequence of alternating gold and platinum-rich regions along <100> in space, with average spacing between centers of A/2. Lattice mismatch shearing strains are caused, for example, by shearing a Pt-rich region over a Au-rich region. The increase in work-hardening rates at small strains is attributed to rapidly increasing deformation-induced internal strains, resulting from shearing, by moving dislocations, of uniformly distributed composition fluctuations in the parent solute lattice. Similar to Cahn's (9) theory, Carpenter related the yield stress to $A^2\lambda$ for both screw and edge dislocations. According to Carpenter (15) the yield stress is given as

$$\sigma = (A\eta)^2 E^2\lambda/2\pi \sqrt{6}Gb \qquad \text{for screw dislocation, and} \qquad (19)$$

$$\sigma = (A\eta)^2 E^2\lambda/2\pi \sqrt{2}Gb \qquad \text{for edge dislocations.} \qquad (20)$$

But both Carpenter (15) and as well as Ditchek and Schwartz (16) neglected the important role of dislocation self stress. As a result their theories cannot be considered to be complete.

Ghista and Nix (17) suggested a dislocation model of the strength of elastically inhomogeneous crystalline materials which is based on the elastic interactions between dislocations and periodic fluctuations of the shear modulus. The model rests on the assumption that the elastic energy of a dislocation in an inhomogeneous material can be treated as if the shear modulus varies radially from the axis of the dislocation. They assumed the variation in the shear modulus to be represented by a Bessel function of the first kind of order either 0 or 1. The variation in the elastic energy of a dislocation with

position in an inhomogeneous material is accounted for by a variable phase factor which is included in the argument of the Bessel functions, the model suggests that the critical stress to initiate plastic flow increases linearly with the amplitude of the shear modulus variation, and varies inversely with the wavelength. They have shown that the critical shear stress required for dislocation movement is

$$\sigma = \left(\frac{P}{\bar{E}}\right)_{max} \bar{G}b \quad \frac{1.75\times10^{-5}}{\lambda} \qquad (21)$$

where, $\bar{G}$ is the average shear modulus, $\bar{E} = \bar{G}b^2$, and P is the force intensity on a dislocation.

But the drawbacks in their theory are as follows:

(i) Consideration of a straight dislocation and neglect of the contribution by the internal coherency stress, and

(ii) even when the Bessel function approximation of the radial variation of the shear modulus is permitted to appear in their theory (18), one cannot rely on their calculations. Since the elastic inhomogeneity is distributed periodically in their model, the self energy should also be a completely periodic function of the position.

Dahlgren (19) determined that the yield strengths were proportional to the difference in cubic lattice parameters of unstressed precipitating phases and independent of other factors such as the precipitate particle size and precipitate volume fractions. The yield stress dependence on lattice parameter differences alone indicated that coherency stresses controlled the yield strengths.

He obtained the yield strength for age hardened spinodal alloys as

$$\sigma = \frac{\bar{m}}{3\sqrt{6}} \; Y \; \frac{\Delta a}{a_o} \tag{22}$$

where, $\bar{m}$ is the Taylor factor, and Δa and a_o are the difference in and the average cubic lattice parameter of the precipitating phases. The equation indicates that the yield strength is dependent only on the internal coherency strains and independent of particle size and precipitate volume fraction. Since Dahlgren (19) assumed a straight dislocation and neglected the effect of dislocation self stress, his theory is not complete.

Hanai et al (20) explained the age-hardening mechanism in spinodal alloys based on the evaluation of an interfacial energy per unit area of the slip plane. They proposed that new interfaces are produced on the slip plane when a crystal with continuous composition fluctuations arising from spinodal decomposition is deformed by slip. They evaluated the energy of such interfaces for modulated structures, and they concluded that the contribution of the interfacial energy is large enough to account for the age-hardening concomitant with spinodal decomposition.

Hanai et al (20) proposed that the yield stress, resulting from the effect of interfacial energy is proportional to the square of the amplitude and to the inverse of the wavelength of the composition modulation for the modulated structure. For the face-centered cubic structure

$$\sigma = (4\sqrt{2}\pi/9) \; \{2U_E \; n_c \; n_s + kG\eta^2\} \; A^2\lambda^{-1} \tag{23}$$

for screw dislocation, and

$$\sigma = (\sqrt{6}\pi/3)\ \{2U_E\ n_c\ n_s + kG\eta^2\}\ A^2\lambda^{-1} \qquad (24)$$

for edge dislocations

where, U_E is the interchange-energy of atom power, n_c is the co-ordination number, n_s is the number of atoms per unit area of the interface and k is a constant related to the shape of the solute rich region.

There are some major drawbacks in the theory of Hanai et al (20). They considered the interfacial energy to be the sum of chemical interfacial energy and elastic strain energy, but interfacial energy is defined per unit area whereas elastic strain energy is defined per unit volume. Secondly, the assignment of interfacial energy to be $0.3J/m^2$ is an overestimation, since the modulated structure in spinodal alloys is characterized by the fluctuation of constitutive atoms and is not brought about by an entirely different atomic arrangement as envisaged in a grain boundary or a twin interface.

Most recently, Kato, Mori and Schwartz (21) used a dislocation force balance equation to consider the incremental stress due to coherency stress in a spinodally modulated structure in face-centered cubic alloys. They considered a mixed dislocation lying mainly in the positive regions of the internal stress field as shown in Figure 3, to be responsible for macroscopic yielding. They argued that the resistance to the motion of the mixed dislocation is the largest of all possible orientations. Edge and screw dislocations will move at lower stresses as predicted by Cahn (9) causing micro-yielding, but inhibited by pinning, will rotate into the mixed orientation which

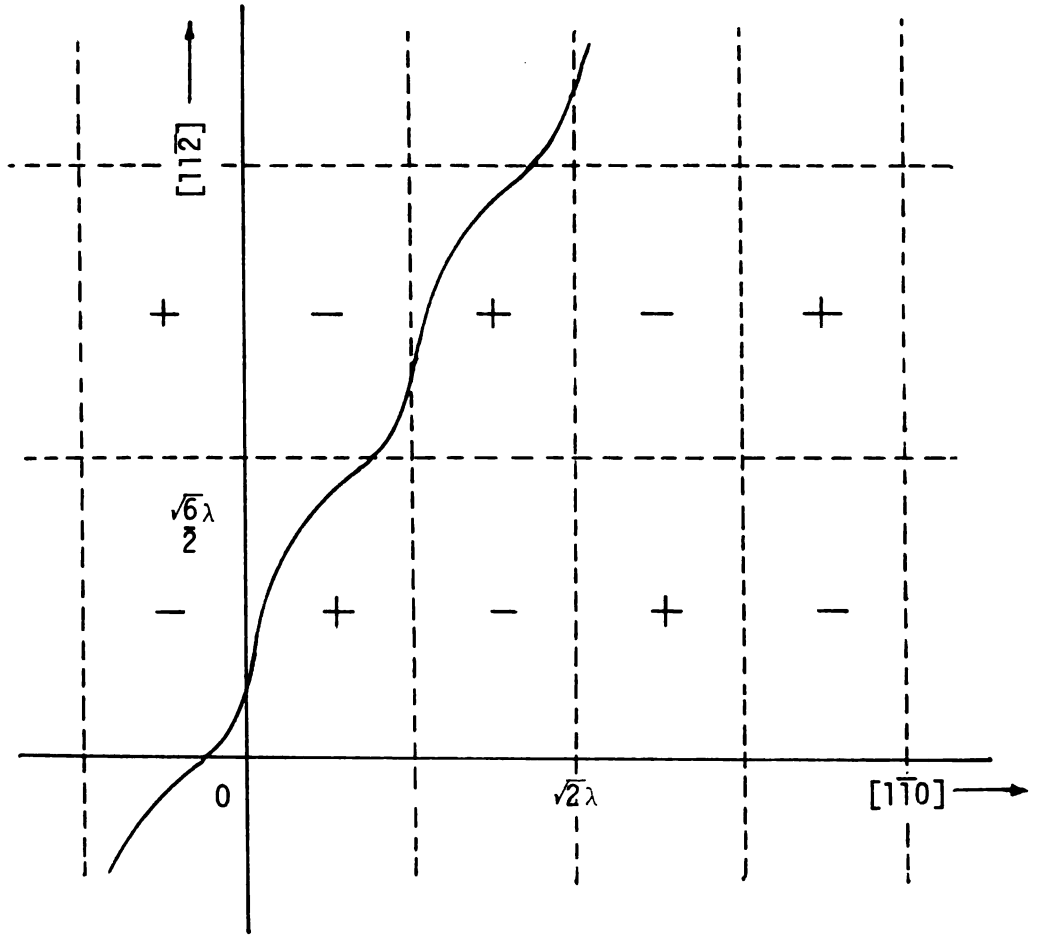

Figure 3: Schematic representation of a mixed dislocation and internal stress profile considered by Kato-Mori-Schwartz. (+, and - positions show respectively maxima and minima of the force acting on the dislocation due to the internal stress.) (21)

suffers the largest resistance. The Kato-Mori-Schwartz theory indicates that the yield stress is given by

$$\sigma = A\eta Y / \sqrt{6} \tag{25}$$

which indicates that it is independent of λ.

In the case of spinodal alloys, as schematically shown in Figure 4, the yielding occurs more gradually in aged than in as-quenched alloys. In analogy to the Pierles-Nabarro yielding, this fact can also be attributed to the difference in the mobility between edge or screw dislocations and mixed dislocations; that is, when the external stress is applied in modulated alloys, screw and edge dislocations move first resulting in micro-yielding. However, due to pinning points, the dislocations eventually acquire an orientation different from the orientations of either edge or screw dislocations and reorient into a mixed orientation. Thus, the macroscopic yield stress is determined by the movement of dislocations with mixed character.

In the case of the Kato-Mori-Schwartz theory, both the predicted linear dependence of the incremental yield stress on $A\eta$ and the magnitude of the incremental yield stress agree well with the experimental results within a factor of two. Considering the uncertainties of the experimental analysis, the agreement is believed to be very good.

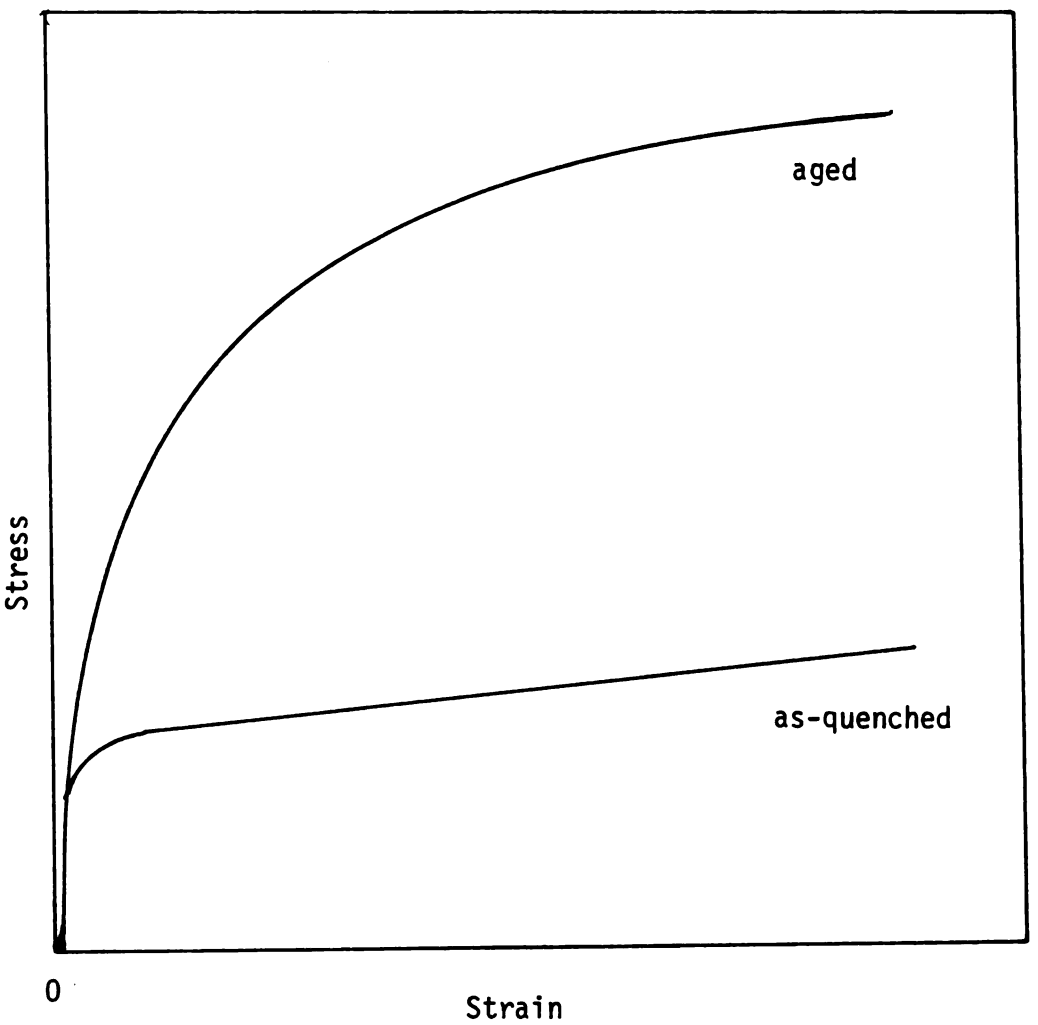

Figure 4: Schematic stress-strain curves in as quenched and aged alloys.

2.3 Single Crystal Studies on Spinodal Alloys

Only a very limited amount of studies have been carried out on single crystals of spinodal alloys. Greggi and Soffa (22) have investigated the flow and fracture stress of Cu-1.07 weight perent Ti spinodal alloy in the form of single crystals. Single crystal tensile specimens with the tensile axis close to the $[\bar{1}23]$ were aged at 673°K for times varying from 10 minutes to 10,000 minutes and tensile tested at room temperature. They found that the critical resolved shear stress increased with aging time but the total strain decreased with aging time. The strengthening of the aged samples was due to the periodic arrays of discrete, coherent precipitates of the metastable Cu_4 Ti phase. They also observed that the samples deformed by primary and as well as secondary slip; they have noticed extensive twinning in the necked region during later stages of the deformation.

2.4 Transmission Electron Microscopic Studies of Spinodal Alloys

Transmission electron microscopy (TEM) has been used to visualize the spinodal microstructure, and to measure the wavelength of composition modulation, waveshape and to analyze dislocation structure. Transmission electron microscopy has demonstrated that spinodal alloys develop a modulated structure. The aging behavior common to many spinodal alloys as examined by the transmission electron microscope, consists of a periodic structure with the periodicity along the <100> directions as predicted by Cahn's theory (8) for anisotropic cubic materials. This is termed as the modulated structure. In addition, this aging behavior shows that the modulated structure

transforms from sinusoidal-shaped in the early stages of the decomposition to square-shaped in the later stages. In the case of the Cu-Ni-Sn spinodal alloy, it is speculated that the composition modulations represent the separation of the as-quenched alloy into Sn-rich and Sn-poor regions; however, the ratio of the atomic percentage of Cu to the atomic percentage of Ni remains the same in both phases.

Transmission electron microscopy studies on the decomposition of Cu-9Ni-6Sn spinodal alloy were carried out by Schwartz, Mahajan and Plewes (23). They investigated the microstructural features of as-quenched and as well as specimens aged at 623°K for various lengths of time. In as-quenched samples they did not observe any structural features that could imply decomposition of the solid solution. They concluded that the glide dislocations tend to dissociate into Shockley partial dislocations, separated by faulted regions and they observed long paired dislocations which they have speculated to be dipoles.

In the case of Cu-9Ni-6Sn samples aged for 5, 40 and 300 minutes, the principal feature observed by Schwartz et al (23) was the appearance of modulated regions which appeared to exhibit some order in their arrangement along <100>; similar structural features have been reported by Butler and Thomas (14) and Livak and Thomas (24) in Cu-Ni-Fe alloys which also decompose spinodally. Regions of discontinuous precipitates interspersed with regions of the modulated structure were observed by Schwartz et al (23) in Cu-9Ni-6Sn specimens aged for eighty hours, and in specimens aged for one hundred and sixty hours, the modulated structure was absent and the only prominent feature was the discontinuous precipitates.

Datta and Soffa (25), in their investigation on the effect of the microstructure on the age-hardening of Cu-Ti spinodal alloys, concluded that the modulated structures which develop in aged alloys result from metastable spinodal decomposition involving the continuous transformation of a single phase into a disordered phase and an ordered phase. They explained the age-hardening response in the alloy in terms of the interaction of dislocations with the internal stress field associated with the spinodal or modulated structures using Cahn's (9) model of spinodal hardening.

The early stages of the spinodal decomposition in Ni-Ti alloys have been studied by Laughlin (26) who reported that a periodic microstructure aligned along the elastically soft directions, namely, <100>. These modulations cannot be considered artifacts since the diffraction patterns show ordering spots around the fundamental spots indicating alternating regions of Ti-rich and Ti-poor phases. The modulations also increase in intensity with aging time. The strain contrast (at constant wavelength) associated with the composition modulations also increases with aging time (27) implying that the amplitude of the modulations also increases.

The precipitation reaction of a high tin phase late in the coarsening stage of the spinodal decomposition of Cu-10Ni-6Sn alloy was studied by Ditchek and Schwartz (28). The indexing of the diffraction ring pattern corresponding to the precipitates suggests that they are incoherent and they have speculated these to be Ni_3Sn, which has a DO_{19} structure (29). The DO_{19} structure is an isotype of the DO_{22} lattice, and is shown in Figure 5.

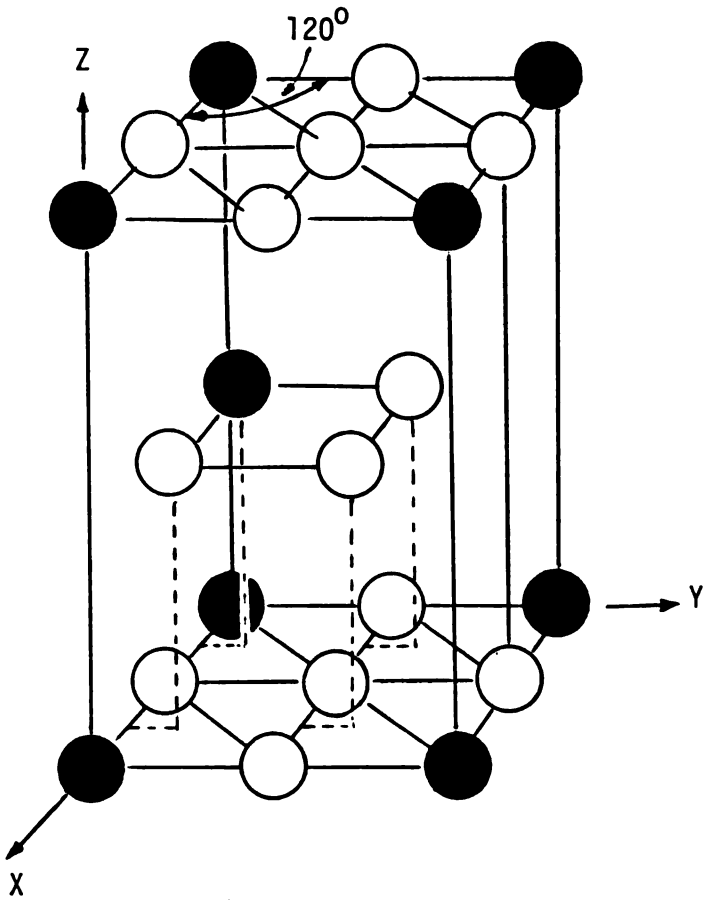

Figure 5: The unit cell associated with the DO_{19}-type superlattice.

○ - Ni

● - Sn

III. PURPOSE OF CURRENT STUDIES

Whereas most of the previous microstructural studies in spinodal alloys were concerned with the modulated structure in aged alloys, the current investigation involves the use of the transmission electron microscopy to determine whether edge and screw dislocations, as predicted by Cahn (9), or mixed dislocations, as predicted by Kato, Mori and Schwartz (21), are responsible for the age-hardening behavior in spinodally decomposed Cu-10Ni-6Sn alloy. Fine grained and as well as large-grained samples were used in these studies.

IV. EXPERIMENTAL PROCEDURE

The Cu-10Ni-6Sn stock for the experimental studies was provided by the Bell Laboratories, [details in Ref. (23)]. The available stock from which the fine-grained and large-grained samples were made was in the form of strips about four millimeters in thickness.

4.1 Fine-Grained Specimens

The fine-grained specimens were prepared by the following steps. The available stock was rolled down to a thickness of about 0.45 to 0.5 millimeters using a cold-rolling mill. Tensile samples with a gage length of 13 millimeters and width of 5 millimeters were cut out as shown in Figure 6. These samples were solution-treated at 1073°K in argon for 3 minutes and then drop quenched into water so as to avoid grain growth. This homogenizing treatment results in the relieving of all stresses induced due to prior mechanical treatments carried out on the samples. The solution treated samples were chemically polished in a solution of 40% nitric acid and 60% distilled water for a short duration to remove any surface contamination. Specimens which were not given any further heat-treatment are referred to as "as-quenched". In order to induce composition fluctuation the alloy some of the specimens were then heat-treated at 623°K in vacuum for periods of 10 minutes, 20 minutes or 60 minutes in a tube-furnace as shown in Figure (7). The specimens were suspended inside the tube using a very fine wire made of manganin.

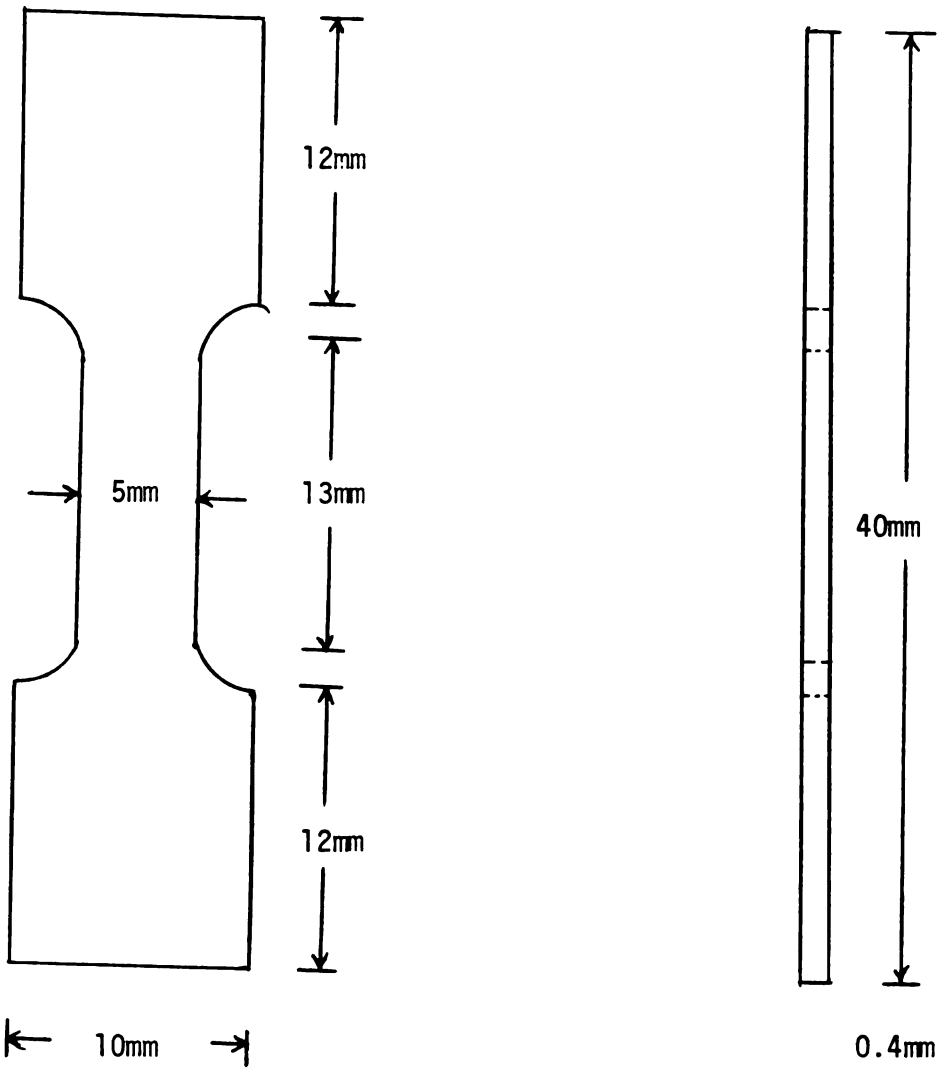

Figure 6: Schematic of the tensile test specimen.

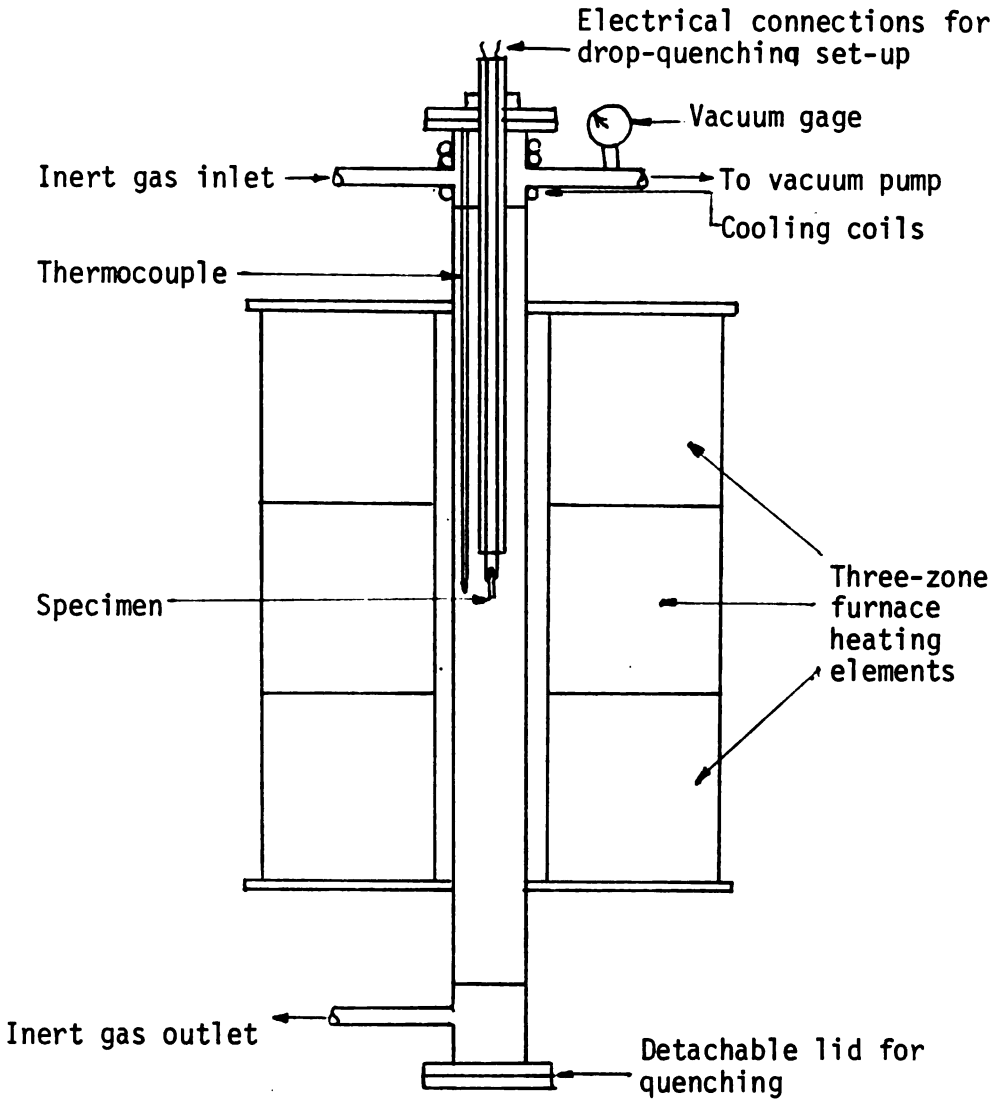

Figure 7: Schematic of tube-furnace used for homogenizing and aging the specimens.

After the aging treatment, the specimens were directly drop-quenched into water by shorting the manganin wire by passing a large current through it. The specimen surfaces were cleaned in a chemical polishing solution of 40% nitric acid and 60% distilled water. The specimens were now deformed in tension in order to induce some strain in the matrix.

The tensile tests on the as-quenched and aged samples were carried out using a micro-tensile fixture attached to the Instron testing machine shown in Figure 8. The specimens were strained to either 5% or 10% plastic strain. The deformed specimens were chemically thinned down to 0.1 millimeter using a solution of 40% nitric acid and 60% distilled water and the surfaces were cleaned using methanol. The gage length was cut into discs of 3 millimeters diameter using a very sharp pair of scissors in order to avoid inducing stresses by the cutting operation.

The central portion of the disc in each case was made transparent to electron beams using a two-step polishing method. The first step, where conditions used are given in Table 1, is known as the "dishing technique" (30), and it was used to produce a preferential polishing in the central region of the specimen using a funnel-shaped apparatus as shown in Figure 9. After polishing for some predetermined time (about 30 seconds) in order to create a shiny dish-shaped concave surface on one side, the specimen was turned over and the polising was continued on the same mode on the other side as well. The main aim of producing concave-shaped surfaces on both sides of the specimen was to produce regions transparent to electrons

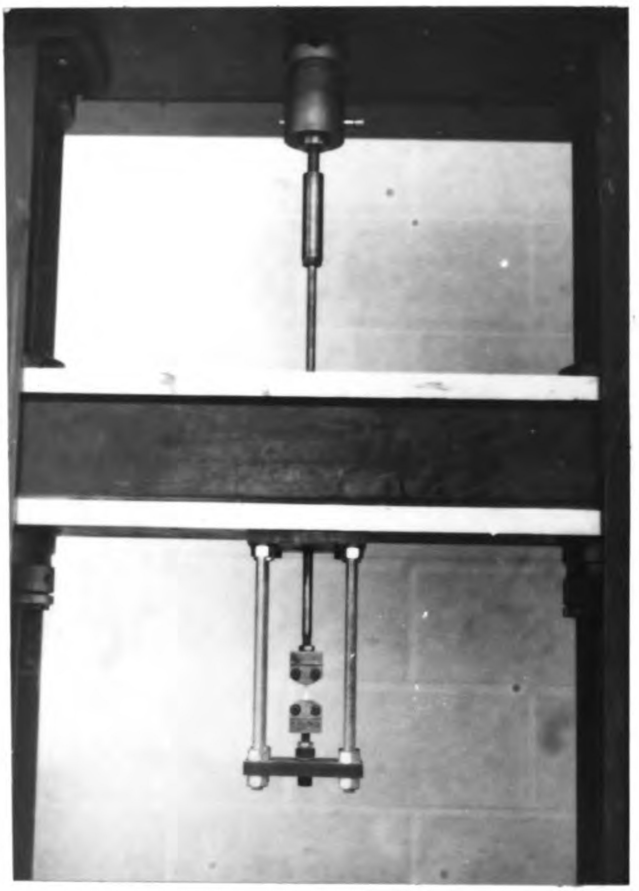

(a)

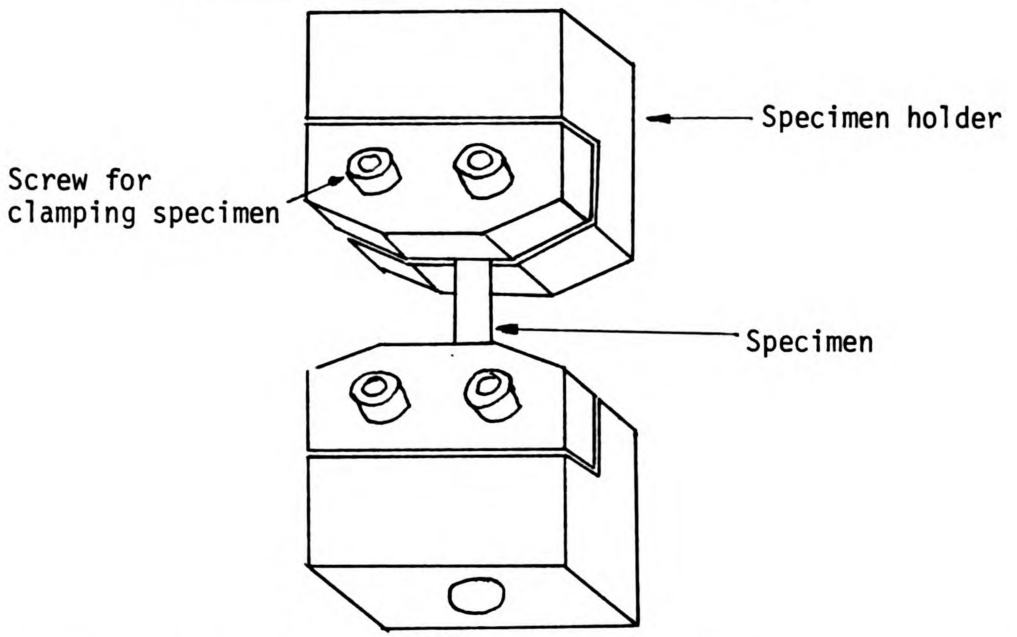

(b)

Figure 8: Microtensile fixture used for testing in Instron testing machine;

a) Photograph.

b) Schematic.

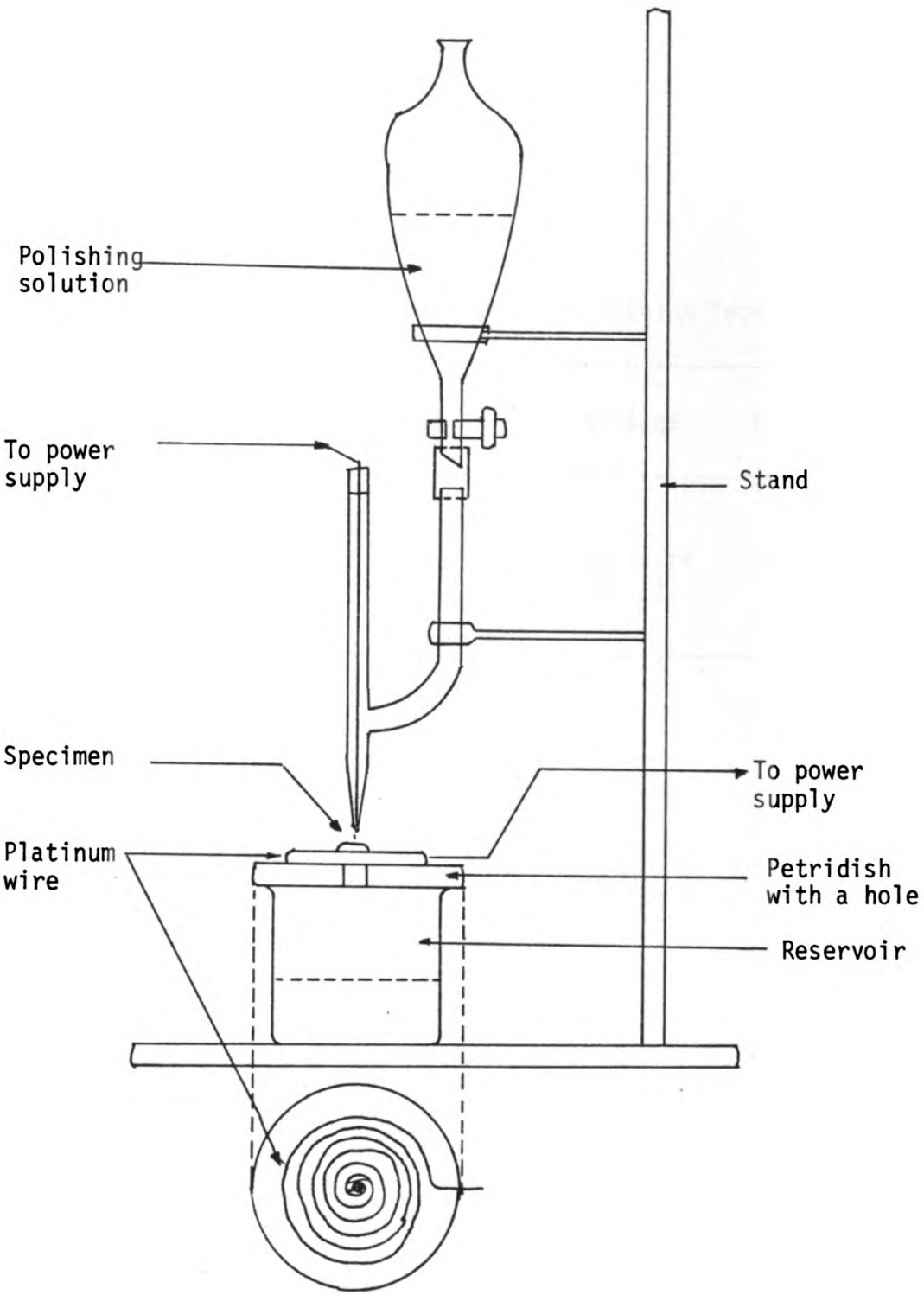

Figure 9: Schematic of the single-jet electropolishing unit.

Table 1: Electropolishing data for "Dishing Technique".

Composition of Electrolyte	Voltage	Temperature
4 parts of Methyl Alcohol plus 1 part of Nitric Acid	50 volts (d.c.)	243^{o} K

in the central portion during the second step of the polishing. In this step, the "dished" specimen was held between circular platinum loops as shown in Figure 10 and electropolished under conditions given in Table 2. The cathode was a cylindrical stainless steel sheet with slots cut out of it. A pointed light source was used to determine when perforation occurred in the center of the foil. The final electropolishing time was usually a few minutes, and as soon as the hole was formed, the sample was removed from the electrolyte and washed thoroughly in running methanol. This procedure was consistently successful in producing then foils suitable for transmission electron microscopic studies.

4.2 Large-Grained Specimens

The large-grained specimens were prepared by the strain annealing method using the following steps. The available stock was rolled down to about a millimeter in thickness and tensile strips were cut out and homogenized at 1073°K for 3 minutes in argon to remove strains due to prior mechanical operations and then drop-quenched in water. These strips were then imparted a critical strain of 8% plastic strain and annealed at 1073°K for 72 hours in vacuum to obtain grain sizes of the order of 1 to 2 millimeters. Samples approximately 4 millimeters wide were then cut out of the large-grained specimens using a diamond saw to induce as little strain as possible. These samples were about 30 millimeters long and they were thinned down to about 0.4 millimeters thickness with emery papers of grades 240, 320, 400 and 600 successively, using a brass-plate substrate. Stresses induced during any of the above operations were relieved by

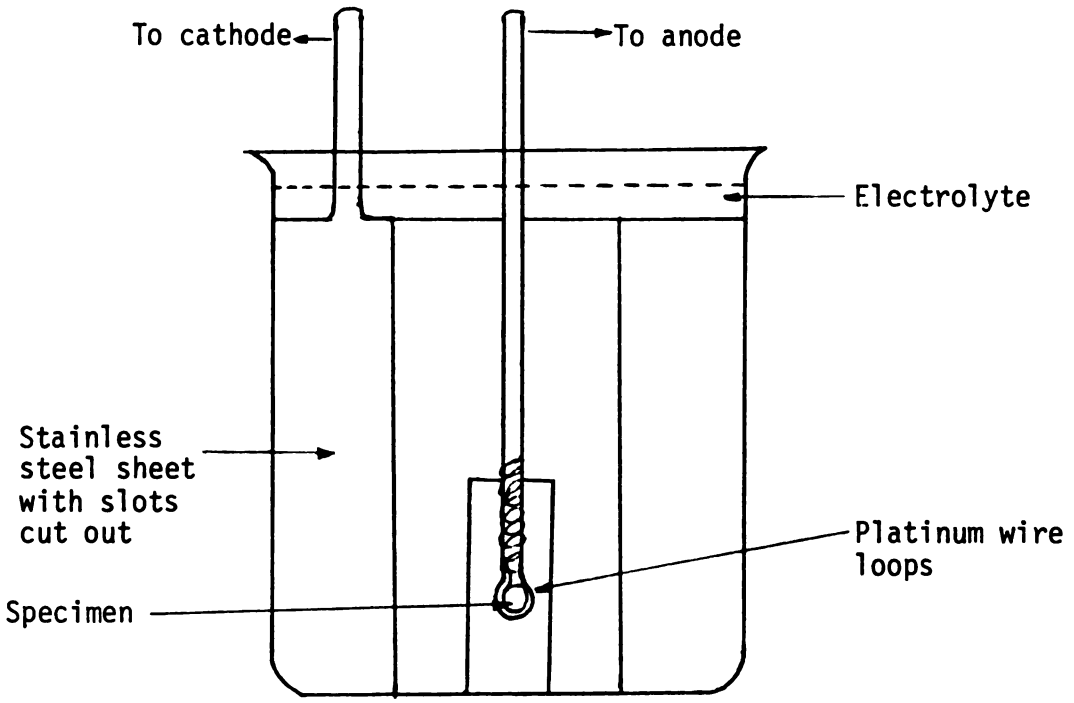

Figure 10: Schematic of final electropolishing unit.

Table 2: Electropolishing data for Final step of thin foil preperation.

Composition of Electrolyte	Voltage	Temperature
4 parts of Methyl Alcohol plus 1 part of Nitric Acid	8 volts (d.c.)	243^{o} K

solution treating the large-grained samples at 1073°K for 6 hours in vacuum followed by drop quenching into water. These samples are, as before, referred to as "as-quenched". Some of the as-quenched specimens were aged at 623°K for 10 and 20 minutes in vacuum in order to induce composition fluctuations.

Surface contamination in the large-grained samples was removed using a chemical polishing solution of 40% nitric acid and 60% distilled water. The as-quenched and as well as the 10 and 20 minutes aged samples were strained to 5% plastic strain using the micro-tensile device shown in Figure 8.

The strained specimens were thinned down chemically to 0.1 millimeter using a 40% nitric acid 60% distilled water solution and cleaned using methanol. Just as in the case of the fine grained specimens, discs of 3 millimeters diameter were cut out and electropolished using the same two-step method used for the preparation of fine-grained foils. The "dishing technique", which was the first step, used conditions given by Table 1, and the final electropolishing, which was the second step, used conditions given by Table 2.

The fine-grained and as well as the large-grained samples were examined in a transmission electron microscope operated at 100 kilovolts.

V. RESULTS AND DISCUSSION

The dislocation structure in fine-grained and large-grained samples of the Cu-10Ni-6Sn spinodal alloy was studied by transmission electron microscopy. The operating voltage of the electron microscope was 100 kilovolts and magnification was varied for the different micrographs by varying the intermediate lens current. The results of the transmission electron microscopic investigations on as-quenched and aged samples are discussed in detail in this section.

5.1 Fine-Grained Specimens

Figure 11 provides the deformation structure in an as-quenched sample that was deformed to 5% plastic strain. It is apparent that there are two slip systems in this particular region and that each has a set of dislocations lying approximately parallel to <112>. The main feature of the dislocations in as-quenched specimens is that they seem to be straight. Figures 12(a) and 12(b) show the dislocation structure of as-quenched samples deformed to 10% plastic strain; whereas Figure 12(a) is the micrograph of a region deformed by single slip with most of the dislocations lying along one direction namely, $[2\bar{1}\bar{1}]$, Figure 12(b) is that of a region deformed in two slip systems, with one set of parallel straight dislocations lying along $[0\bar{1}1]$ and the other set of parallel straight dislocation lying along $[2\bar{1}1]$. Besides having straight dislocations, the micrographs of the as-quenched specimens do not show any modulated structure due to spinodal decomposition, as expected, and dislocation densities seem

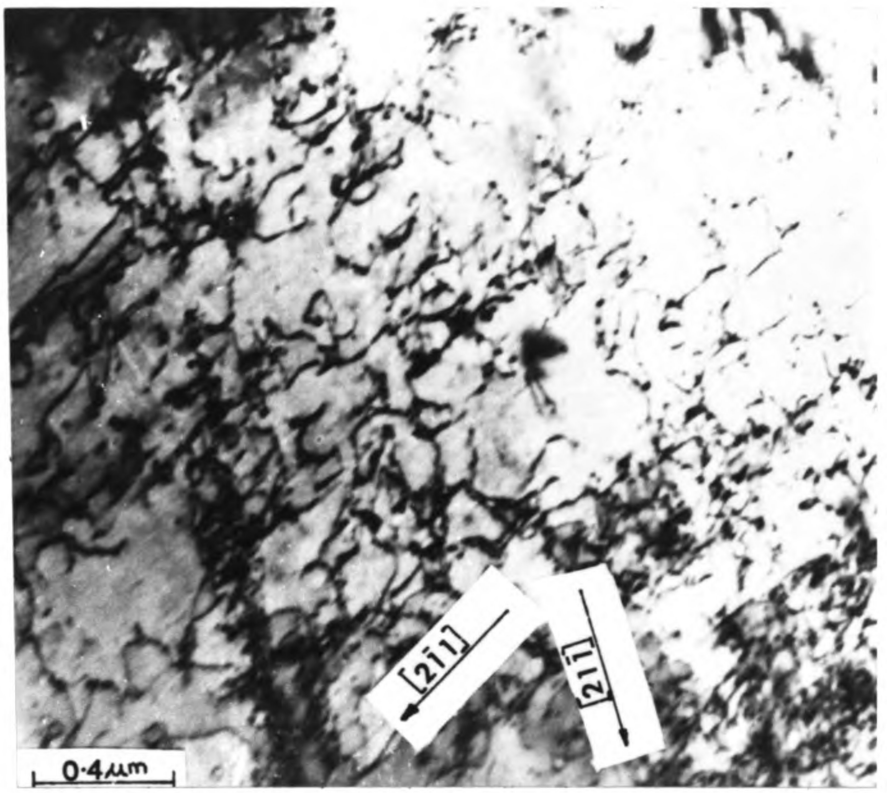

Figure 11: Dislocation structure in a fine-grained as-quenched specimen deformed by 5%. The foil normal is near [011].

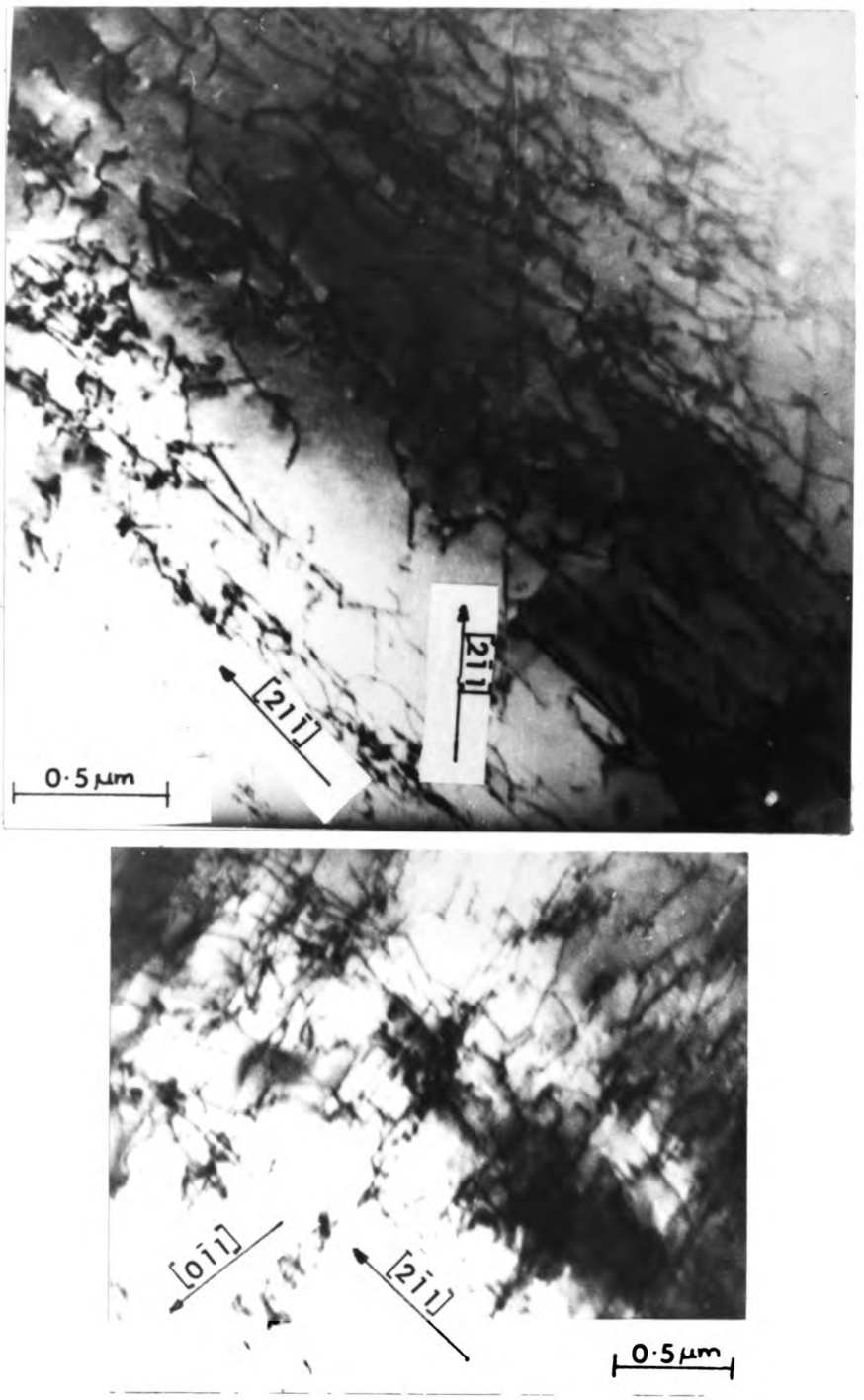

(a)

(b)

Figure 12: Deformation structure in fine-grained as-quenched specimens after 10% deformation. Foil normal is near [011] for both micrographs.

to be quite high indicating that dislocation multiplication in homogenized specimens is relatively easy.

Figures 13(a) and 13(b) show the deformation structure of specimens aged for 10 minutes at 623°K and deformed by 10% plastic strain. The modulated structure due to spinodal decomposition is visible in both of these micrographs and it is obvious that the contrast due to the composition modulation interferes with the contrast due to the dislocations. The dislocations still appear to be mostly straight, though some of them appear to be curved. In Figure 13(a) the dislocations are present on the (111) slip plane, and hence appear to be long, with a set of them lying parallel to the [101] direction whereas Figure 13(b) shows two sets of parallel dislocations, lying along $[2\bar{1}\bar{1}]$ and $[0\bar{1}\bar{1}]$. The striking feature in the micrographs of the 10 minute aged samples as compared to the micrographs of the as-quenched samples is a significant lowering in the density of the dislocations, apparently due to the interference of the strain field associated with the dislocations by the strain field associated with the modulated structure.

Figures 14(a) and 14(b) represent the dislocation structure of specimens aged at 623°K for 20 minutes and deformed by 5% and 10% plastic strain, respectively. The most important features that can be noticed in these micrographs are the clearly visible modulated structure due to spinodal decomposition and a large number of dislocations which appear to be curved unlike in the case of the deformed as-quenched specimens. This suggests that mixed dislocations may be responsible for the hardening in spinodally

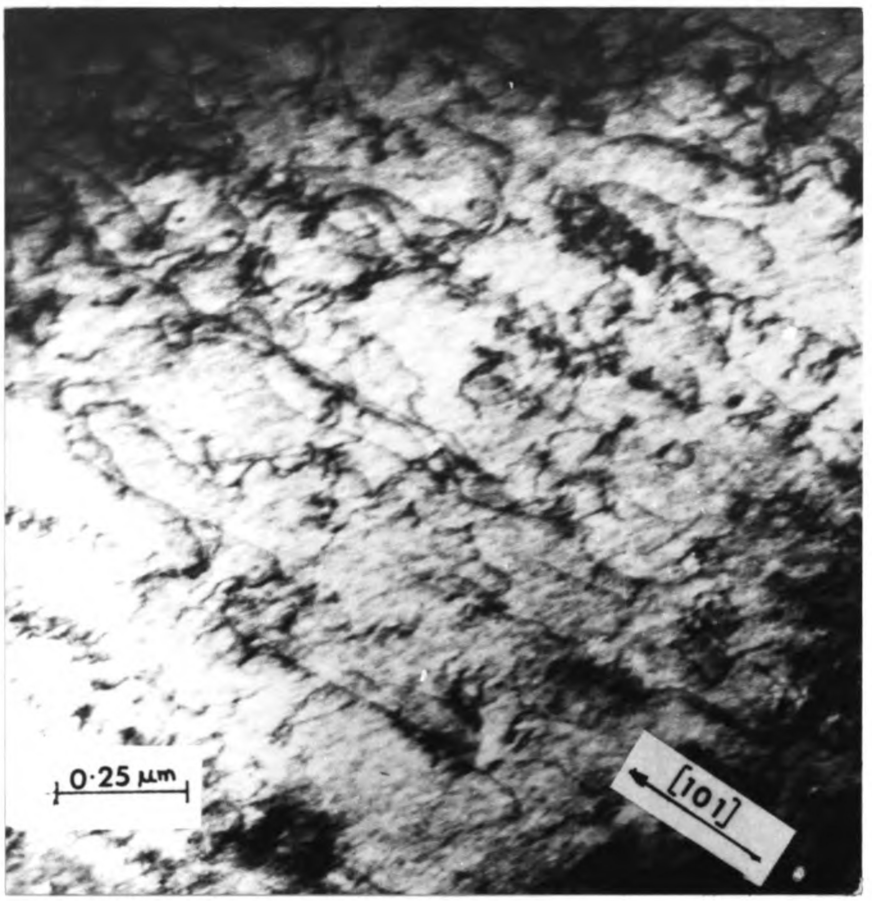

(a)

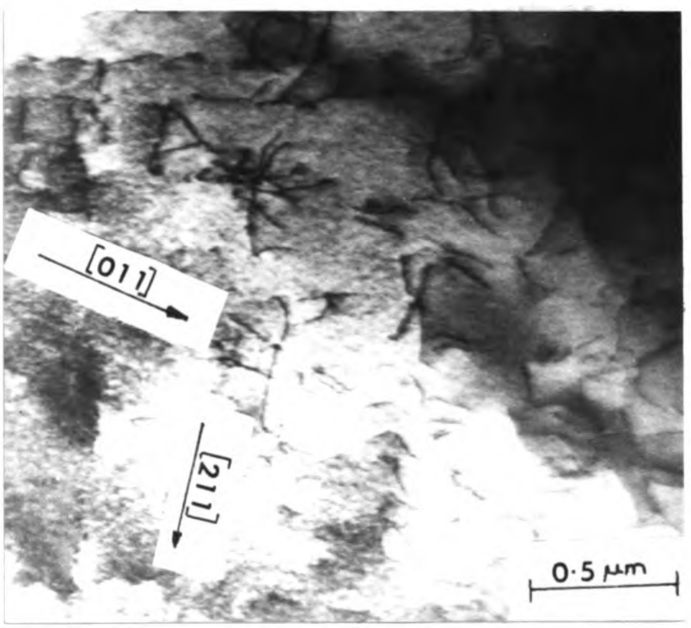

(b)

Figure 13: Dislocation structure in fine-grained specimens aged for 10 minutes at 623° K and deformed by 10%. Foil normal is near [$\bar{1}$11] for (a) and [011] for (b).

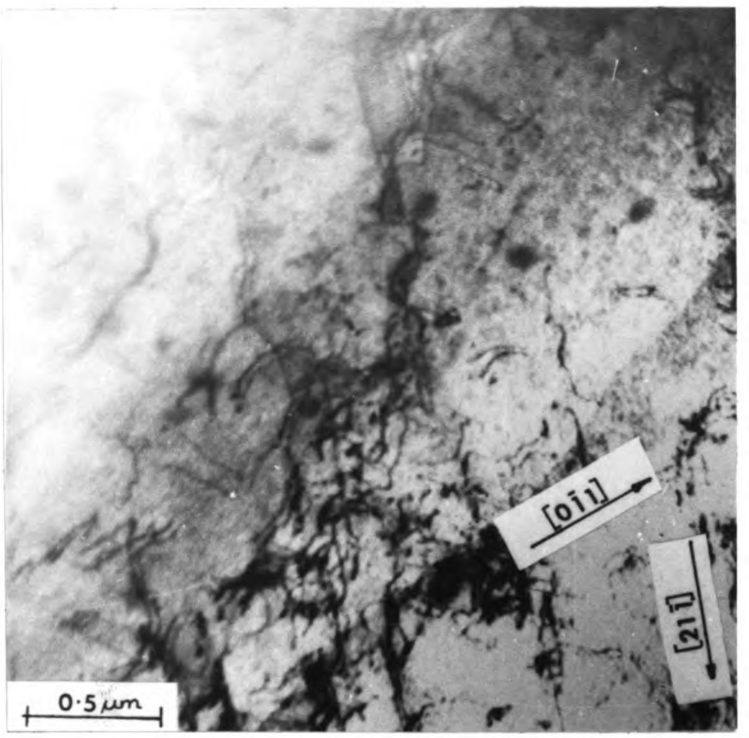

(a)

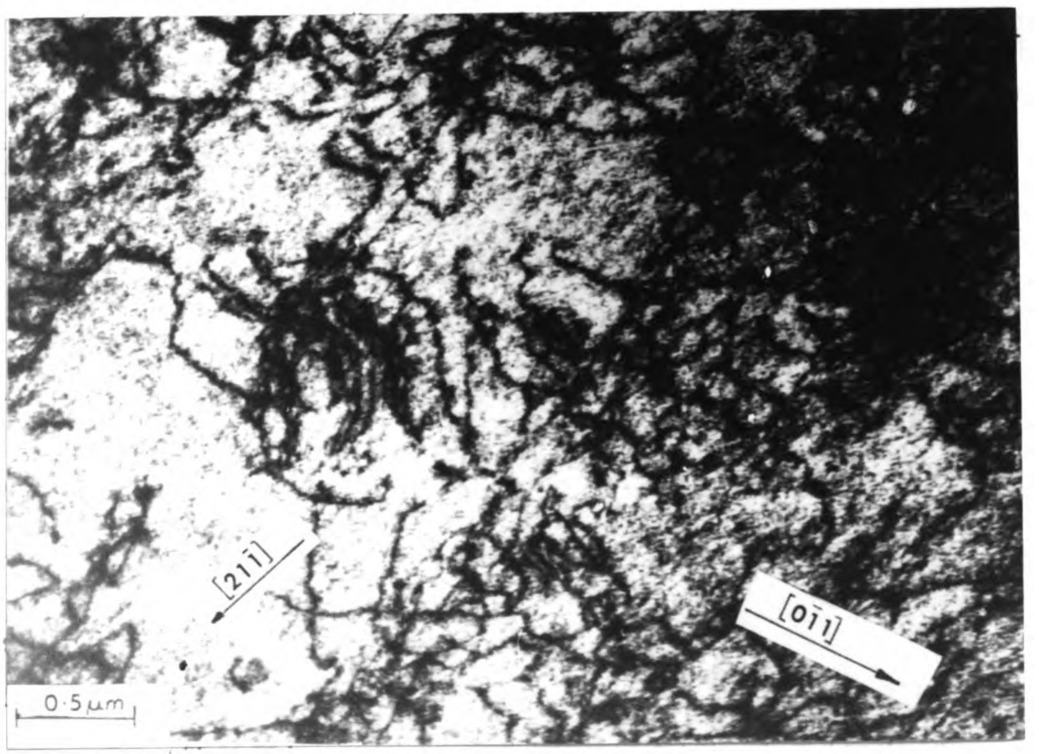

(b)

Figure 14: Dislocation structure in fine- grained specimens aged for 20 minutes at 623°K. Foil normal is near [011] for both micrographs.

a) After 5% deformation. b) After 10% deformation.

modulated structures. In Figure 14(b) the dislocations seem to be pinned at various points which is evidenced by the observation that these dislocations do not appear to be smooth lines. It is also obvious that the contrast due to the modulated structure interferes with the dislocation contrast.

Micrographs of dislocation structure in specimens aged for one hour at 623°K and deformed by 5% and 10% are presented in Figures 15(a) and 15(b), respectively. The few dislocations that are visible are curved indicating once again that mixed components may play a significant role in the hardening of spinodally modulated structures. The contrast due to the modulated structure is so strong that the dislocations are hardly visible, apparently due to the strain field of the modulated structure interfering with the strain field of the dislocations. The tremendous decrease in dislocation density as compared to as-quenched specimens also indicates that dislocation multiplication is difficult in heavily modulated structures.

It was felt that the dislocation-structure could not be observed in specimens aged for longer than one hour. However, a fine-grained specimen aged at 623°K for 24 hours in vacuum was examined in the transmission electron microscope. Figure (16) shows spherical particles along the grain boundaries, and they might be due to the precipitation reaction of a high tin phase late in the coarsening stage of the spinodal decomposition (28). The diffraction ring pattern corresponding to these precipitates was indexed, and it was found to be from crystal of body centered cubic structure.

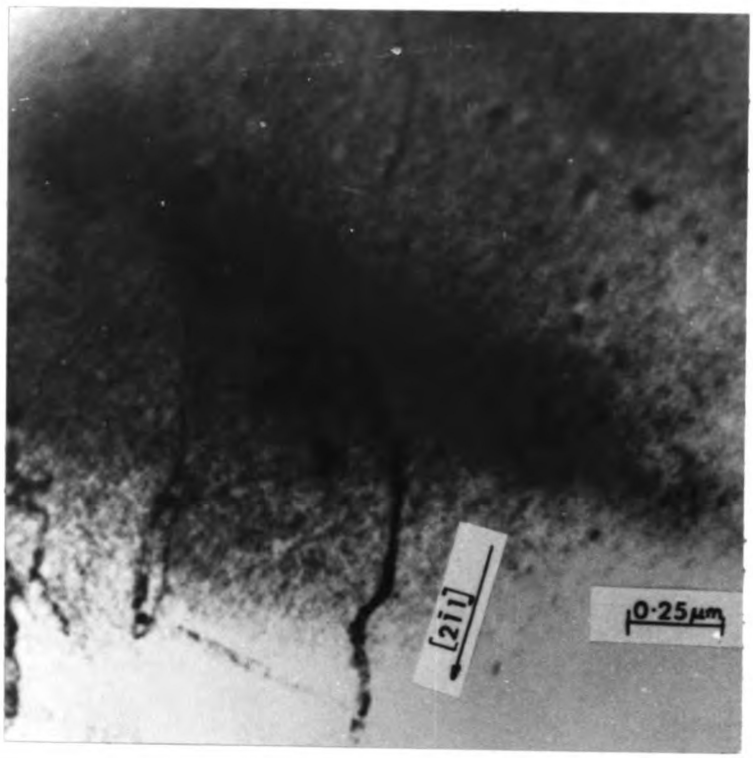

(a)

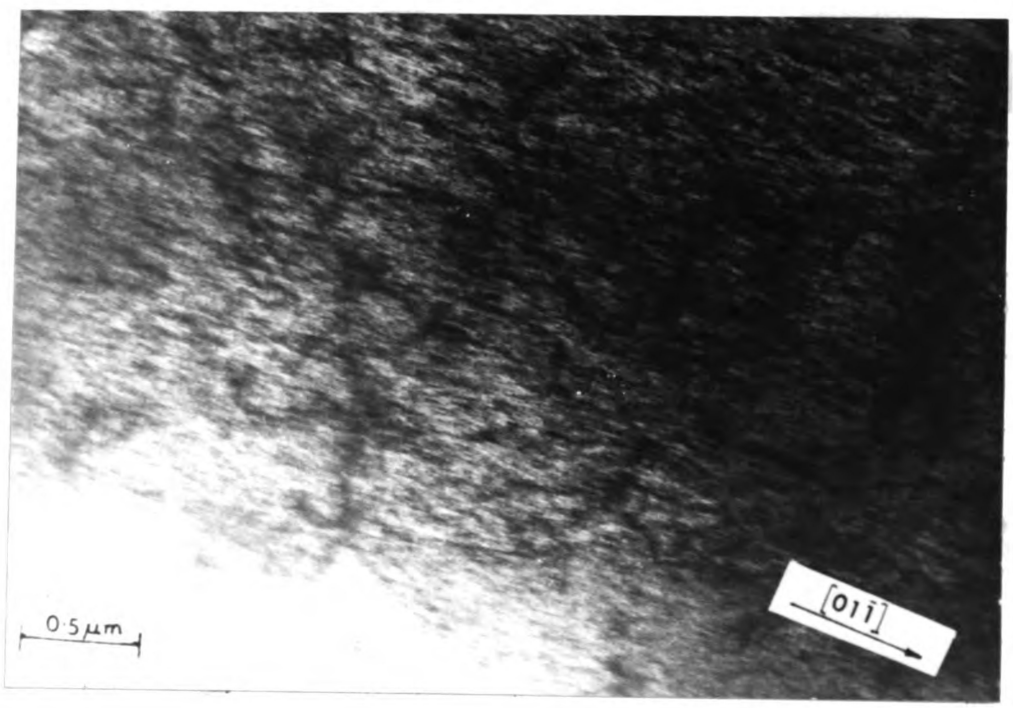

(b)

Figure 15: Dislocation structure in fine-grained specimens aged for 1 hour at 623°K. Foil normal is near [011] for both micrographs.

a) After 5% deformation. b) After 10% deformation.

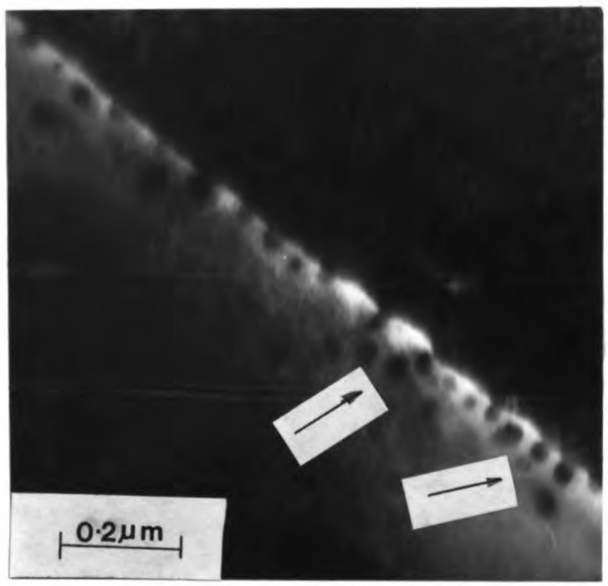

Figure 16: Grain-boundary precipitates in a fine-grained specimen aged for 24 hours at 623°K.

Another important observation was the appearance of ordering spots around fundamental spots in aged samples and these were absent in the diffraction patterns of homogenized specimens. These ordering spots may be due to the ordering of the tin rich phase in the spinodally decomposed alloy.

5.2 Large-Grained Specimens

Although fine-grained specimens can provide information about age hardening in spinodally modulated structures, they are far from ideal to obtain crystallographic information about the dislocation structure. Deformation structures in a large-grained as-quenched specimen are presented in Figures 17(a), 17(b) and 17(c). The prime features are the absence of the modulated structure, and long straight dislocations, present in various {111} planes. The other {111} slip planes are at an angle to the foil surface. The dislocations present in these {111} slip planes which are slanted to the foil normal are projected as straight lines. All dislocations are parallel to the <110> directions and this feature is quite different from the observations made in fine-grained specimens. As expected from the micrographs of fine-grained as-quenched samples, the dislocations are neither curved nor wavy.

In the microstructures of large-grained specimens aged at 623°K for 10 minutes and deformed by 5% plastic strain presented in Figures 18(a) and 18(b) and some straight dislocations and some dislocations with sharp bends are observed. The modulated structure due to spinodal decomposition is also evident. In Figures 19(a) and 19(b), most of the dislocations present are curved and there are

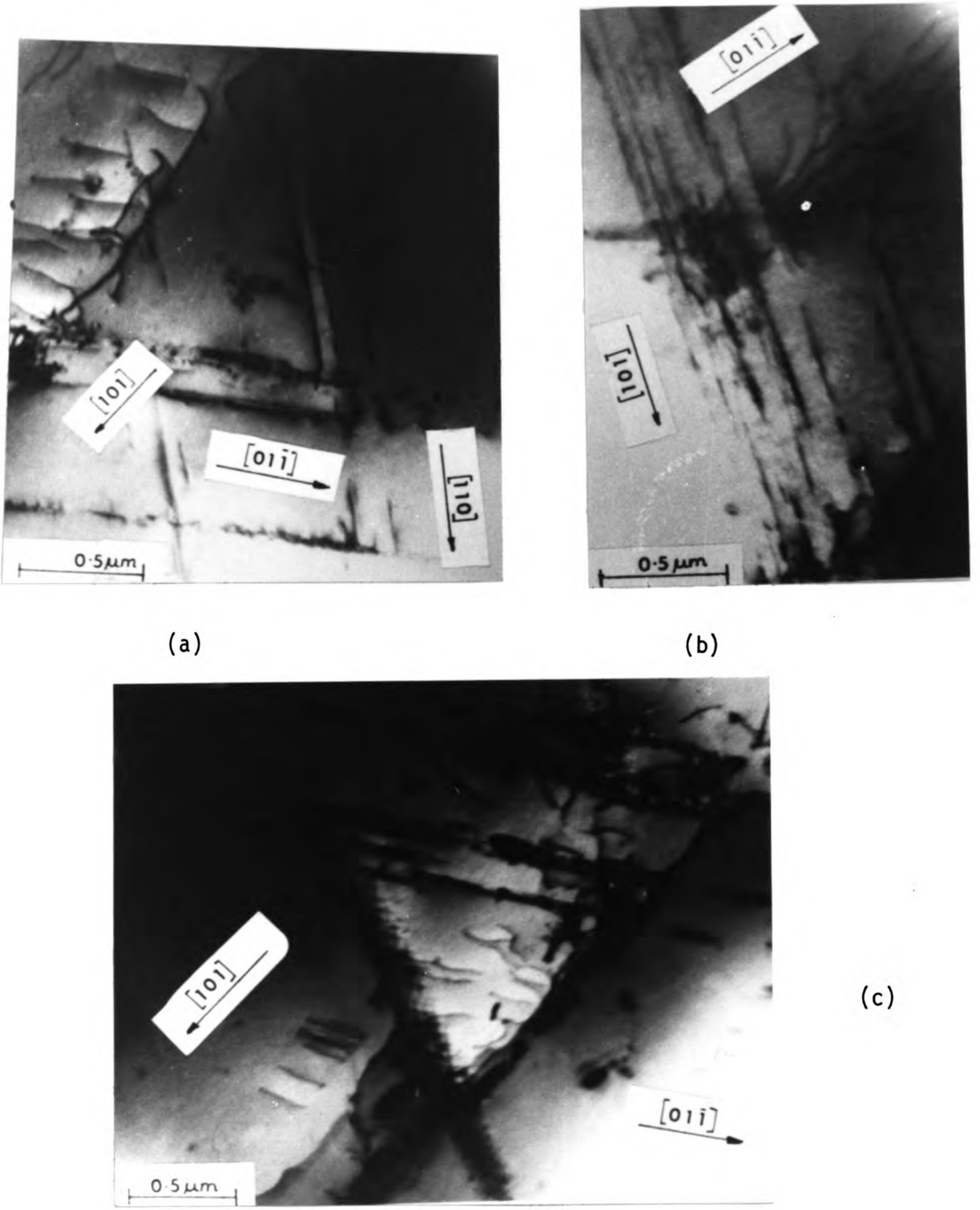

Figure 17: Dislocation structure in a large-grained as-quenched specimen after 10% deformation. Foil normal is near [111] for all three micrographs.

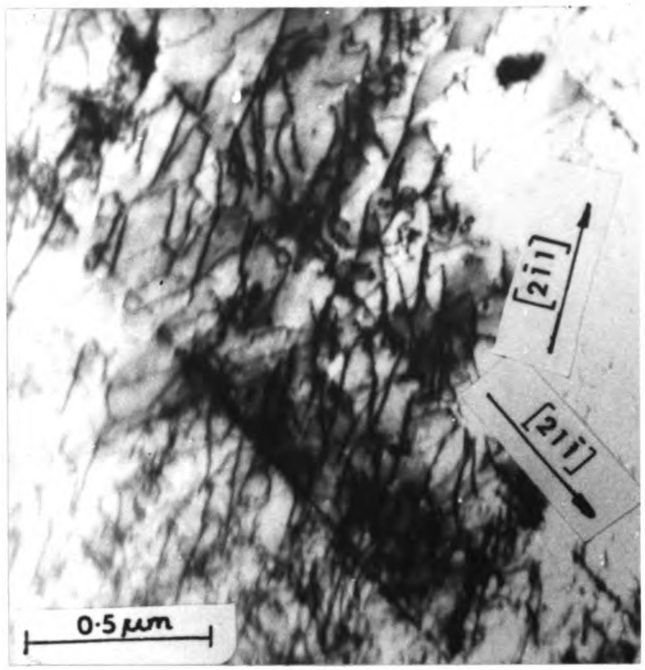

(a)

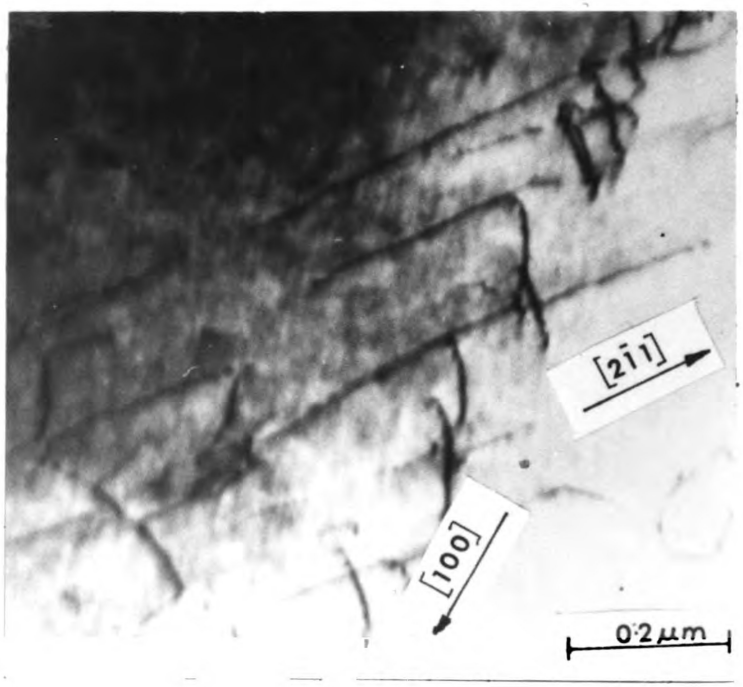

(b)

Figure 18: Dislocation structure in a large-grained specimen aged at 623°K for 10 minutes and deformed by 5%. Foil normal is near [011] for both micrographs.

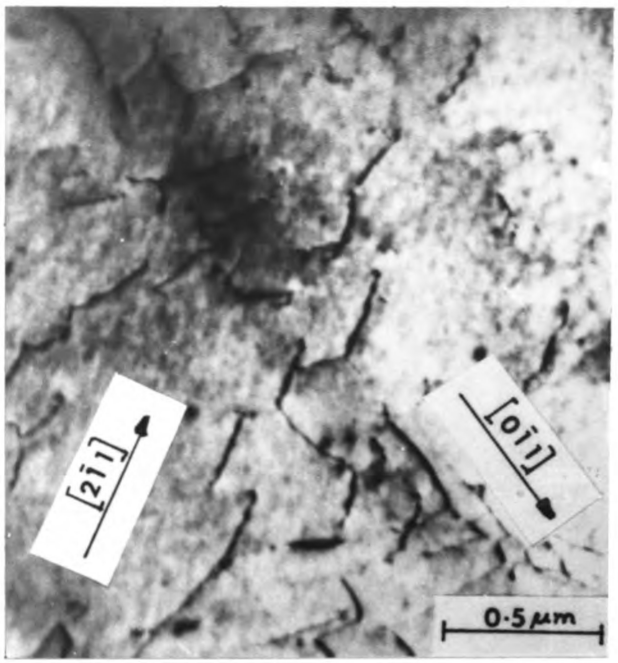

(a)

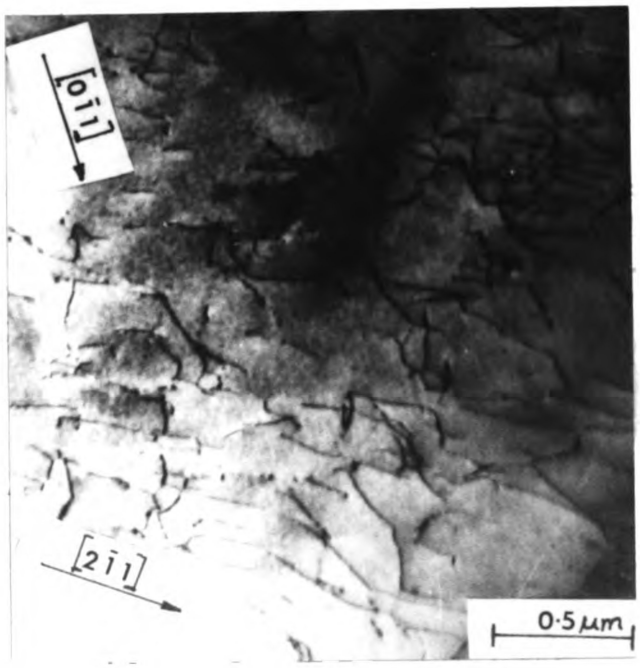

(b)

Figure 19: Dislocation structure with sharp bends and cusps in the dislocations in a large-grained specimen aged at 623°K for 10 minutes and deformed by 5%. Foil normal is near [011] for both micrographs.

sharp bends and cusps in them, apparently due to the dislocations interacting with the modulated structure.

Figures 20, 21, 22 and 23 illustrate the dislocation structure in large-grained samples aged at 623°K for 20 minutes and deformed by 5% plastic strain. Most of the dislocations present are curved indicating that the mixed components may be playing a significant role in the deformation of such specimens. Further, significant decrease in dislocation density in the active slip planes (compared to as-quenched specimens) indicates that the dislocation multiplication is difficult in aged specimens. Wavy shaped dislocations observed in Figure 21 suggest that they are held back at various points, but the wavelength of these wavy dislocations, measured to be about 1,000Å in Figure 21(a) does not correspond to the measured wavelength of the compositional modulation in aged Cu-10Ni-6Sn alloy as reported by Ditchek and Schwartz (28). They differ by an order of magnitude. Sharp bends and cusps are observed in the dislocations shown in Figures 22(a), 22(b), and 22(c), and dislocation dipole like appearance caused by pinning and folding of dislocations are observed in Figure 22(a). It can also be noted that the dislocations in this set of micrographs are not smooth. They appear to be wavy but the wavelength in this case is an order of magnitude less than the ones observed in Figure 21, and correspond very well to the measured wavelength of the composition fluctuation by Ditchek and Schwartz (28).

In order to analyze the character of the dislocations responsible for the age-hardening in the spinodally modulated structure, specimens

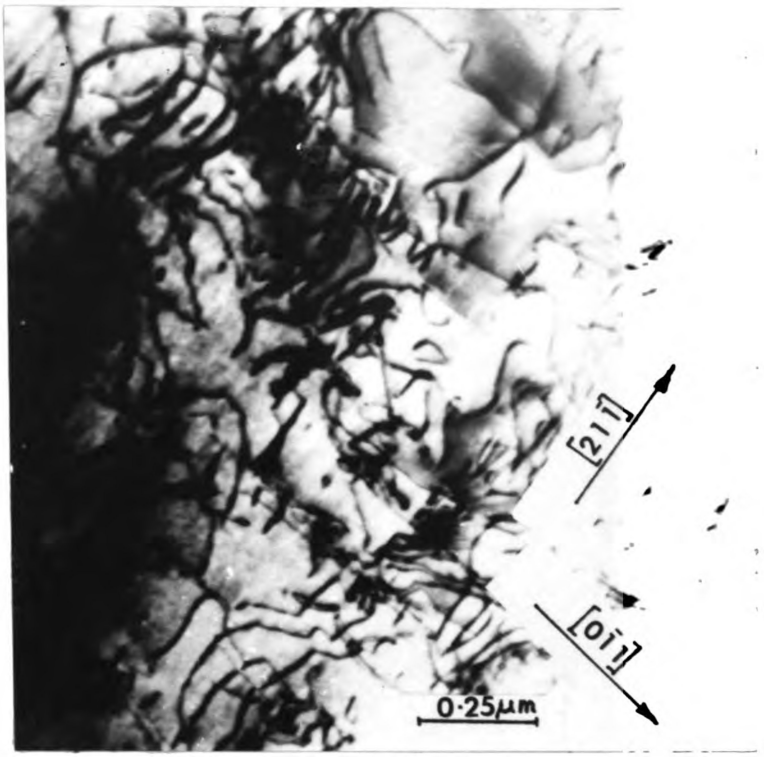

(a)

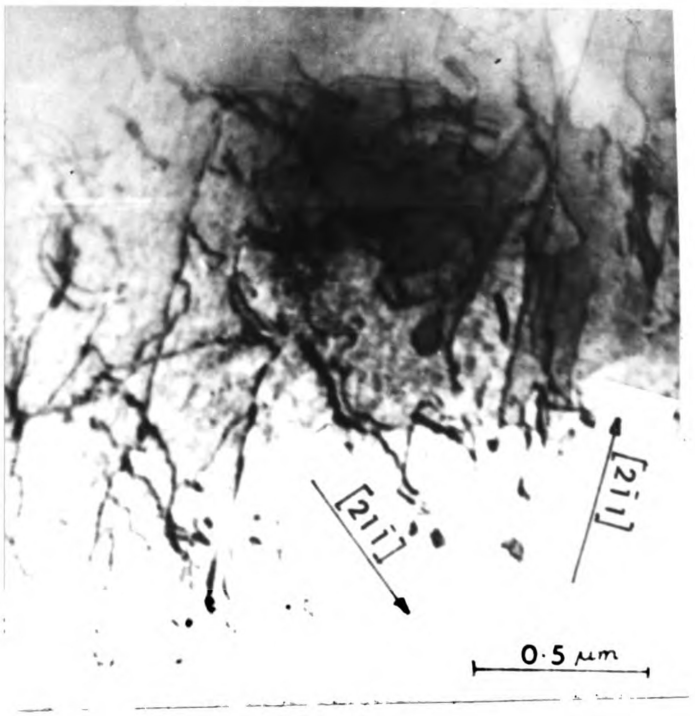

(b)

Figure 20: Dislocation structure in large-grained specimens aged at 623°K for 20 minutes and deformed by 5%. Foil normal is near [011] for both micrographs.

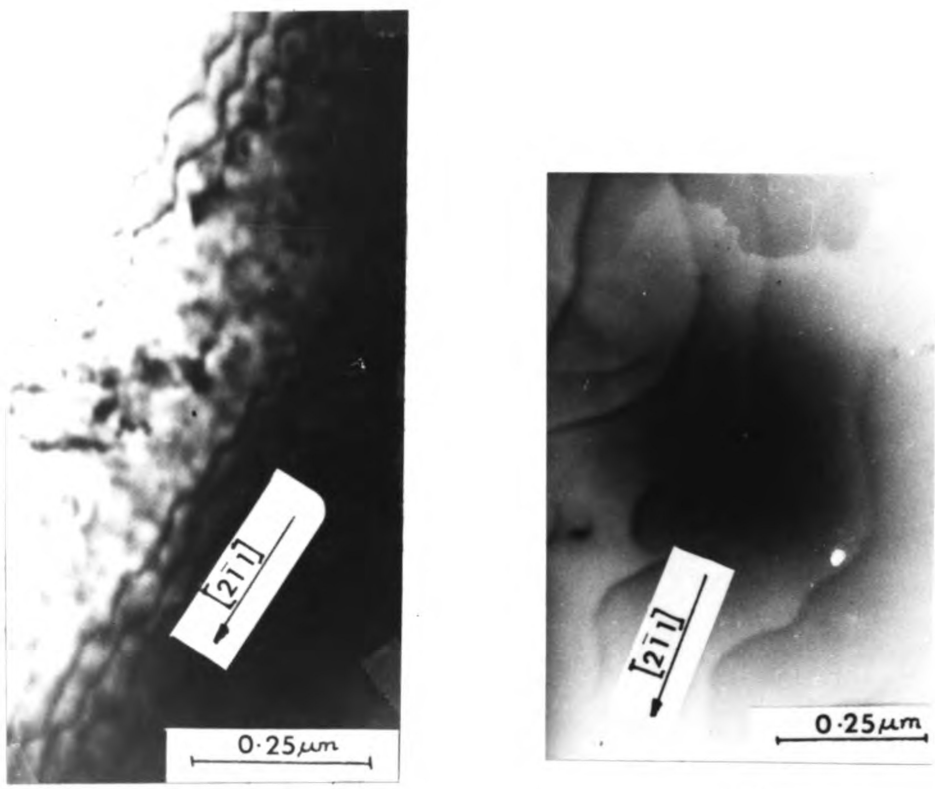

(a) (b)

Figure 21: Wavy-shaped dislocations observed in large-grained specimens aged at 623°K for 20 minutes and deformed by 5%.

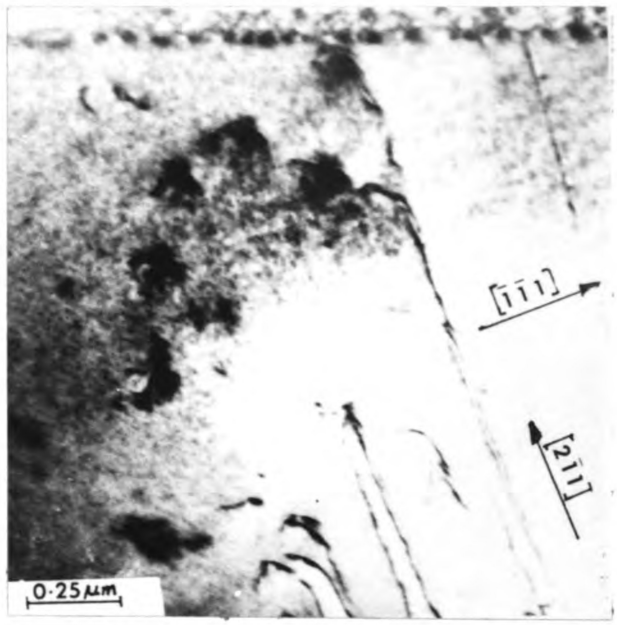

(a)

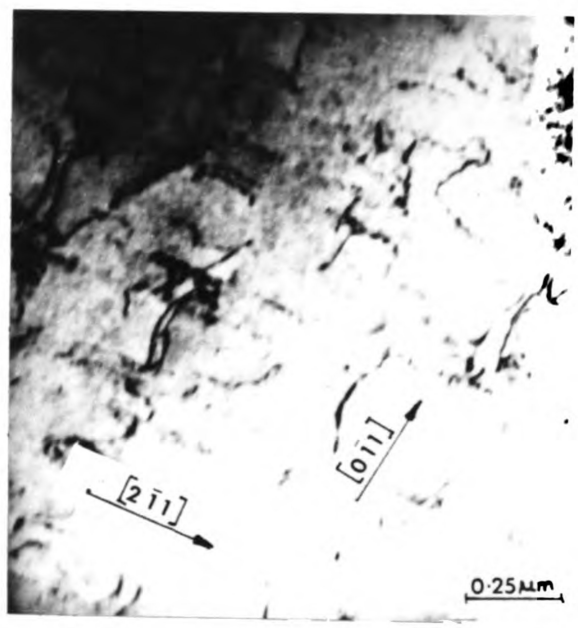

(b)

Figure 22: Sharp cusps and bends in dislocations observed in large-grained specimens aged at 623°K for 20 minutes and deformed by 5%. Foil normal is near [011] for all four micrographs.

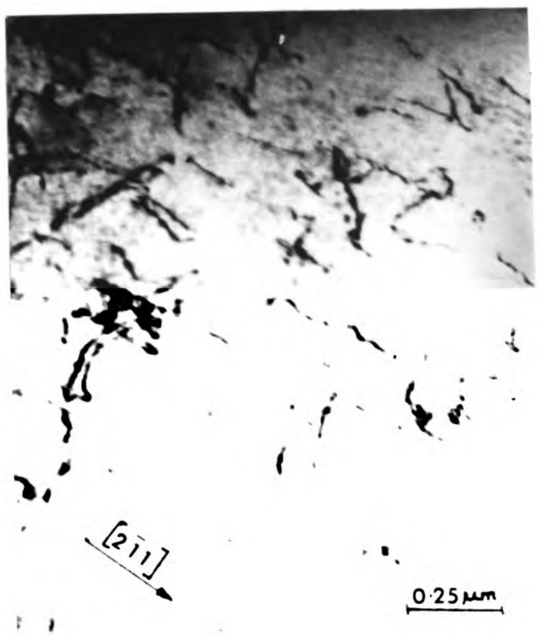

(c)

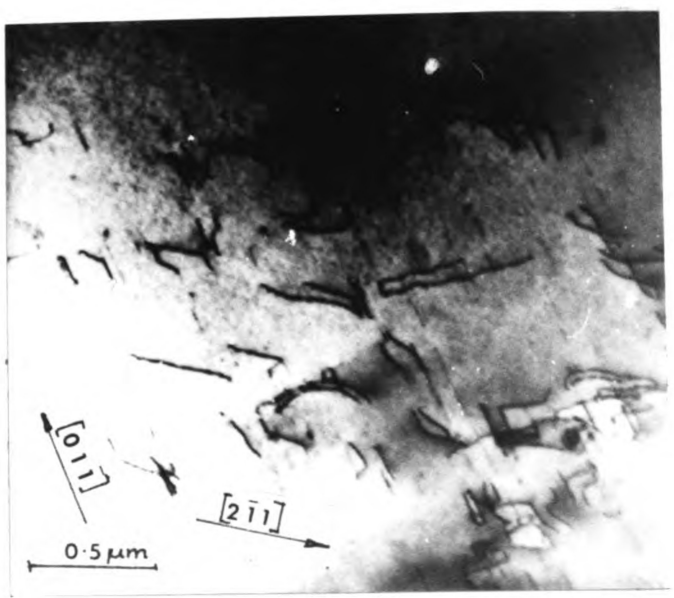

(d)

Figure 22: (Continued).

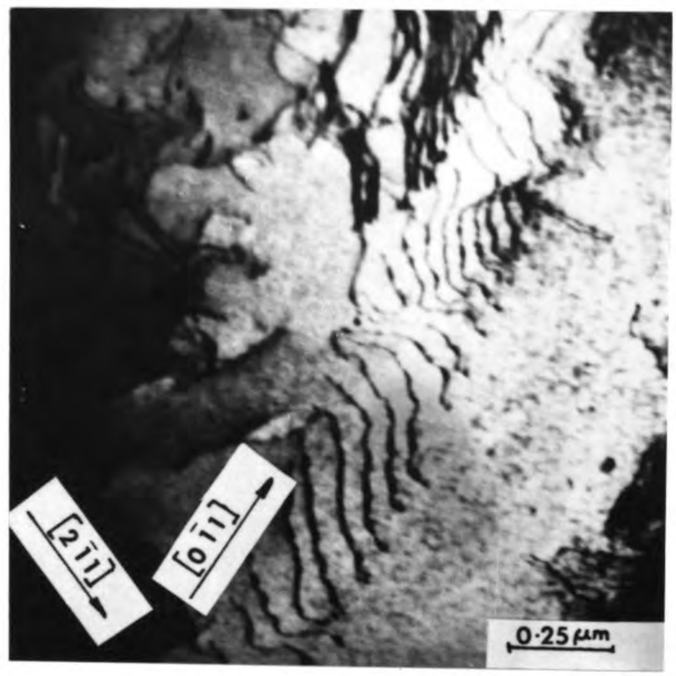

(a)

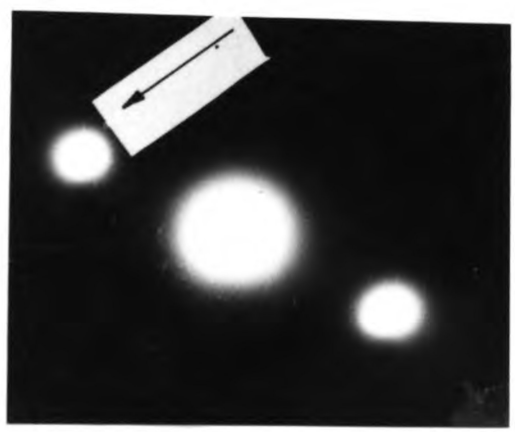

(b)

(c)

Figure 23: Curved dislocations present in a large-grained specimen aged at 623°K for 20 minutes and deformed by 5%.

a) Bright field image. b) Diffraction pattern.

c) Dark field image corresponding to diffraction spot indicated by the arrow.

cut from a large-grained sample aged at 623°K for 20 minutes and deformed to 5% plastic strain were examined in a Philips EM 300 electron microscope operated at 100 kilovolts. This microscope had a stage with tilting (±50°) and rotating (350°) capabilities. Such an arrangement enabled the dislocation Burgers vector analysis by $\vec{g}.\vec{b}$ method, where $\vec{g}$ is a vector normal to the reflecting plane, and $\vec{b}$ is the Burgers vector of the dislocation. According to this method, the dislocation goes out of contrast when $\vec{g}.\vec{b}$ is equal to zero and is in contrast when $\vec{g}.\vec{b}$ is not equal to zero. By tilting and rotating the specimen appropriately a series of micrographs was taken with the $\vec{g}$ vector near [211], [112] and [110] respectively, as shown in Figures 24(a), 24(b) and 24(c). One particular dislocation, which is in contrast only in Figure 24(a) (indicated by A) but out of contrast in Figures 24(b) and 24(c), was analyzed. This analysis is summarized in Table 3. As can be seen from the analysis, the Burgers vector of this dislocation is along $[1\bar{1}0]$. When the projections of the <110> directions are analyzed for the [211] plane normal, they strongly suggest that this particular dislocation lies along [011], and the other dislocations along corresponding <110> directions. The above observations strongly indicate that dislocation A is of mixed character, which lies along the [011] direction in the plane containing [211] and $[0\bar{1}1]$ directions. This is in strong agreement with the Kato-Mori-Schwartz theory (21), which considers that mixed dislocations which lie, on the average, parallel to <110> and to be responsible for the age hardening of the spinodally modulated structure.

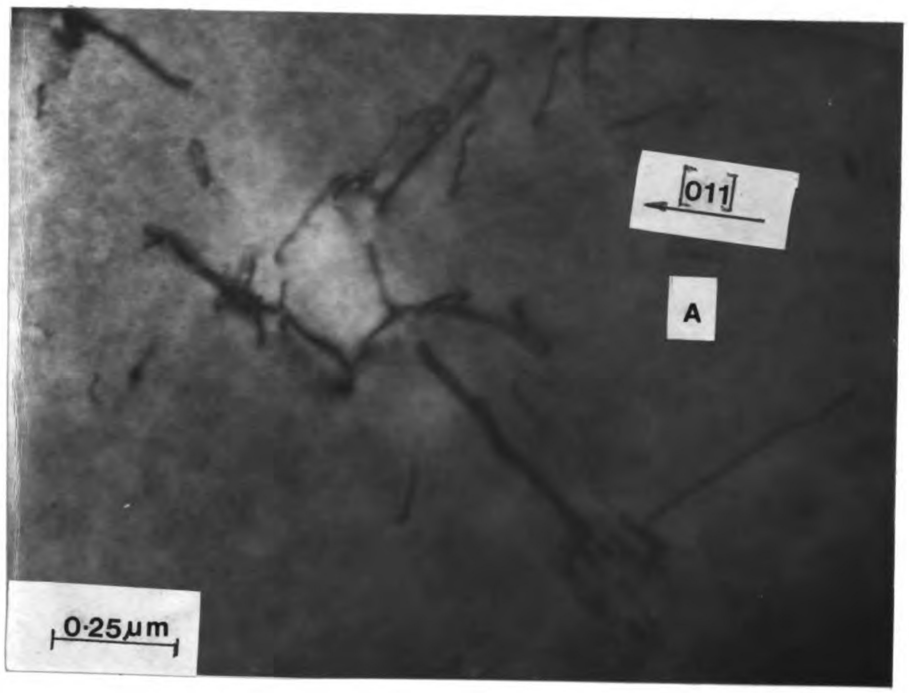

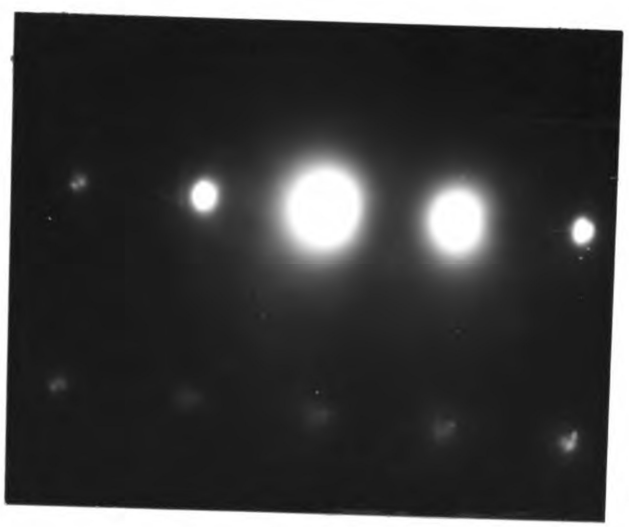

Figure 24: (a) Dislocation structure in a large-grained specimen aged at 623°K for 20 minutes and deformed by 5%. $\vec{g}$ = [211].

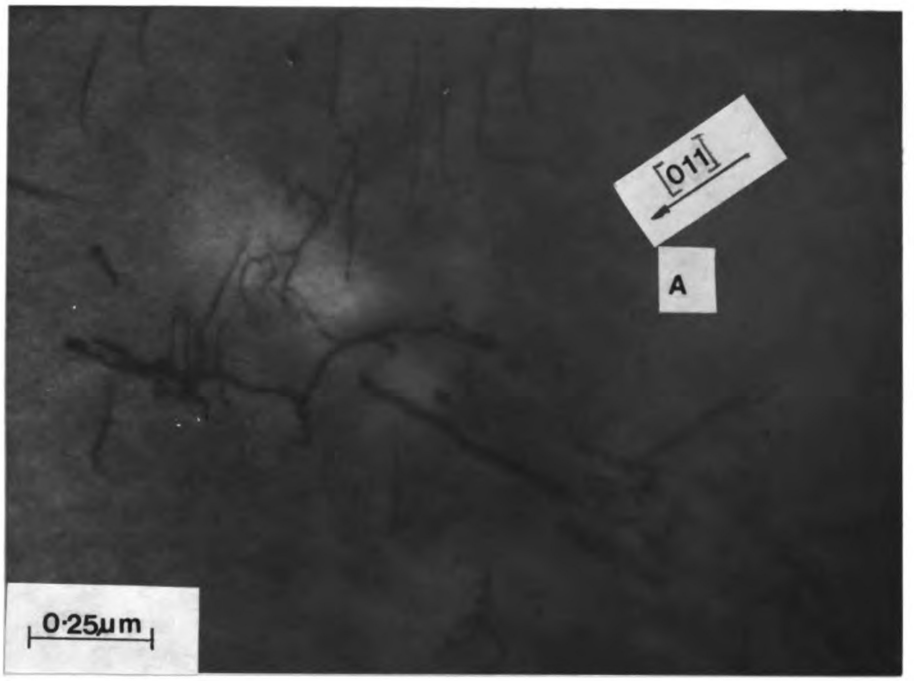

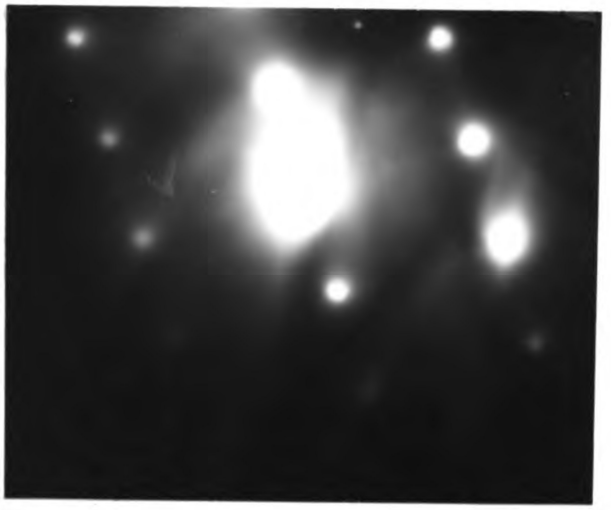

Figure 24: (b) Same region as Figure 24 (1). $\vec{g}$ = [112].

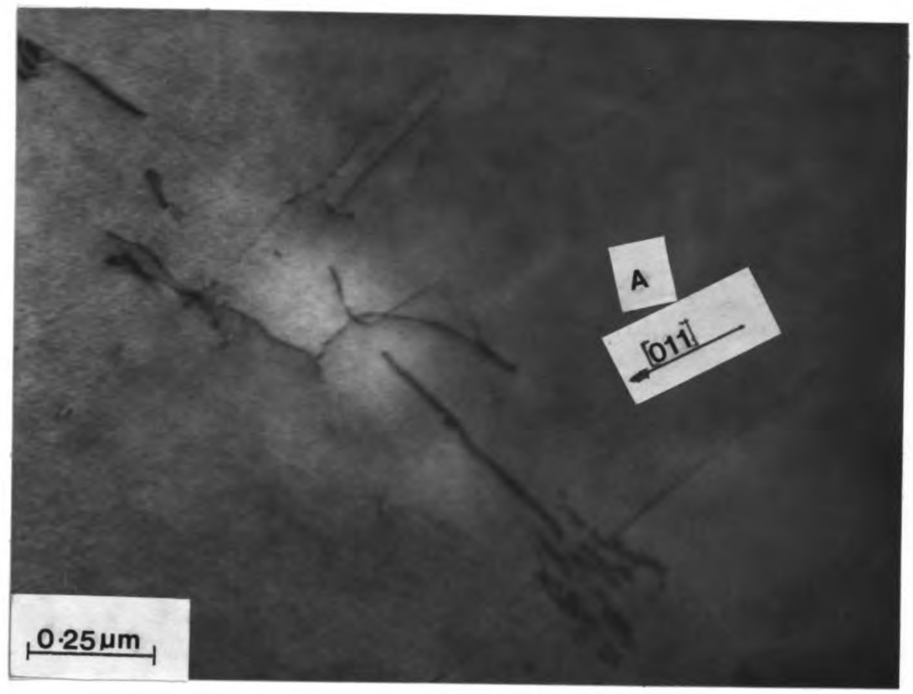

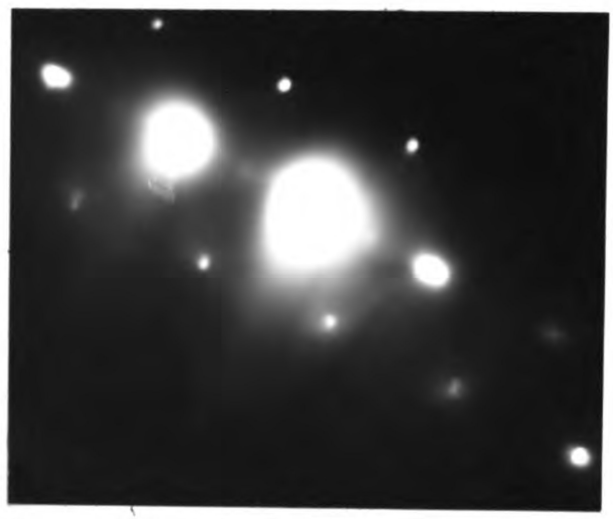

Figure 24: (c) Same region as Figure 24 (1). $\vec{g}$ = [110].

Table 3: Possible values of $\vec{g}.\vec{b}$ for the dislocations under the three reflections in Figures 24 (a), (b) and (c).

Figure Number	$\vec{g}$ \ $\vec{b}$	$\frac{1}{2}[101]$	$\frac{1}{2}[110]$	$\frac{1}{2}[011]$	$\frac{1}{2}[\bar{1}01]$	$\frac{1}{2}[1\bar{1}0]$	$\frac{1}{2}[01\bar{1}]$	Dislocation Contrast A
24 (a)	[211]	$\frac{3}{2}$	$\frac{3}{2}$	1	$-\frac{1}{2}$	$\frac{1}{2}$	0	Visible
24 (b)	[112]	$\frac{3}{2}$	1	$\frac{3}{2}$	$\frac{1}{2}$	0	$-\frac{1}{2}$	Invisible
24 (c)	[110]	$\frac{1}{2}$	1	$\frac{1}{2}$	$-\frac{1}{2}$	0	$\frac{1}{2}$	Invisible

VI. CONCLUSIONS

Results of the transmission electron microscopy to analyze the dislocation structure in as-quenched and aged specimens of the Cu-10Ni-6Sn spinodal alloy, of both fine-grained and large-grained types, can be summarized as follows:

(i) Deformation structure of aged specimens contains more curved dislocations compared to the straight dislocations in deformed as-quenched specimens. This suggests that mixed components may play a significant role in the deformation of aged specimens.

(ii) Dislocations present in deformed aged specimens have sharp cusps and bends indicating that they are pinned at various points. This feature is not observed in as-quenched specimens.

(iii) Dislocation density in aged specimens is significantly lower than in as-quenched specimens that have undergone the same amount of deformation. This observation suggests that dislocation multiplication from active sources is hampered in the modulated structure; as a result sources present in other regions of the specimen have to become active to accommodate the deformation.

(iv) There have been some observations in which the dislocation in aged specimens appear to be wavy and their wavelength is of same order of magnitude as the measured wavelength of compositional modulation in this alloy.

(v) Use of large-grained samples (as compared to fine-grained specimens) significantly helps in the analysis of the dislocations since the entire region of observation is usually within one large grain.

(vi) A $\vec{g}.\vec{b}$ analysis on a deformed large-grained sample indicated mixed dislocations which lie parallel to <110> to be responsible for the age hardening of the spinodally modulated structure. This is in strong agreement with the Kato-Mori-Schwartz theory (21).

REFERENCES

1. Cahn, J. W., "Spinodal Decomposition," Trans. AIME, 242, 166-180, (1968).

2. Ditchek, B. and Schwartz, L. H., "Application of Spinodal Alloys," Annual Review of Materials Science, 9, 219-253, (1979).

3. Nicholson, R. B. and Tufton, P. J., "Precipitation Procedures of Hard Magnetic Materials," Z. Angew Physik, 2, 59-62, (1966).

4. Gibbs, J. W., Collected Works, 1, (New Haven: Yale University Press, 1948), p. 105 and p. 252.

5. Hillert, M., "A Solid-Solution Model for Inhomogeneous Systems," Acta Metall, 9, 525-535, (1961).

6. Hilliard, J. E. and Cahn, J. W., "Free Energy of a Non-Uniform System," J. Chem. Phys., 28, 258-267, (1958).

7. Cahn, J. W., "On Spinodal Decomposition," Acta Metall, 9, 795-801, (1961).

8. Cahn, J. W., "On Spinodal Decomposition in Cubic Crystals," Acta Metall, 10, 179-183, (1962).

9. Cahn, J. W., "Hardening by Spinodal Decomposition," Acta Metall., 11, 1275-1281, (1963).

10. Fleischer, R. L., "Solution Hardening by Interaction of Impurity Gradients and Dislocations," Acta Metall., 8, 32-35, (1960).

11. Fleischer, R. L., "Effects of Non-Uniformities on the Hardening of Crystals," Acta Metall., 8, 598-604, (1960).

12. Douglass, D. L. and Barbee, T. W., "Spinodal Decomposition in Al/Zn Alloys," J. Mater. Sci., 4, 121-129, (1969).

13. Lefevre, B. G., D'Annessa, A. T., and Kalish, D., "Age-Hardening in Cu-15Ni-8Sn Alloy," Met. Transactions, 9A, 577-586, (1978).

14. Butler, E. P. and Thomas, G., "Structure and Properties of Spinodally Decomposed Cu-Ni-Fe Alloys," Acta Metall., 18, 347-365, (1970).

15. Carpenter, R. W., "Deformation and Fracture of Gold-Platinum Polycrystals Strengthened by Spinodal Decomposition," Acta Metall., 15, 1297-1308, (1967).

16. Ditchek, B. and Schwartz, L. H., Proceedings of the Fourth International Conference on Strength of Metals and Alloys, 3, 1319, (1976).

17. Ghista, D. N. and Nix, W. D., "A Dislocation Model Pertaining to the Strength of Elastically Inhomogeneous Materials," Mat. Sci. and Eng., 3, 293-298, (1968/69).

18. Dahlgren, S. D. Ph.D. Thesis, University of California, Berkeley, CA, (1966).

19. Dahlgren, S. D., "Correlaton of Yield-Strength with Internal Coherency Strains for Age-Hardened Cu-Ni-Fe Alloys," Met. Transactions, 8A, 347-351, (1977).

20. Hanai, Y., Miyazaki, T., and Mori, H., "Theoretical Estimation of the Effect of Interfacial Energy on the Mechanical Strength of Spinodally Decomposed Alloys," J. Mater. Sci., 14, 599-606, (1979).

21. Kato, M., Mori, T., and Schwartz, L. H., "Hardening by Spinodal Modulated Structure," Acta Metall., 28, 285-290, (1976).

22. Greggi, J., and Soffa, W. A., "Preliminary Observations of the Flow and Fracture of Cu-Ti Alloy Single Crystals Containing Coherent Precipitates," Scripta Metall., 12, 525-529, (1978).

23. Schwartz, L. H., Mahajan, S., and Plewes, J. T., "Spinodal Decomposition in a Cu-9wt. % Ni- 6wt % Sn Alloy," Acta Metall., 22, 601-609, (1974).

24. Livak, R. J. and Thomas, G., "Spinodally Decomposed Cu-Ni-Fe Alloys of Asymmetrical Compositions," Acta Metall., 19, 497-505, (1971).

25. Datta, A. and Soffa, W. A., "The Structure and Properties of Age-Hardened Cu-Ti Alloys," Acta Metall., 24, 987-1001, (1976).

26. Laughlin, D. E., "Spinodal Decomposition in Nickel Based Ni-Ti Alloys," Acta Metall., 24, 53-58, (1976).

27. Laughlin, D. E. and Cahn, J. W., "Spinodal Decomposition in Age-Hardened Cu-Ti Alloys," Acta Metall., 23, 329-339, (1975).

28. Ditchek, B., and Schwartz, L.H., "Diffraction Study of Spinodal Decomposition in Cu-10w/oNi-6w/oSn," Acta Metall., 28, 807-822, (1980).

29. Barret, C. and Massalski, T. B., "Structure of Metals," 3rd Edition, (McGraw-Hill, U.S.A, 1966) p. 278.

30. Hirsch, P. B., Howie, A., Nicholson, R. B., Pashley, D. W., and Whelan, M. J., "Electron Microscopy of Thin Crystals," (Butterworths, London, 1965) p. 36.